Interactions between magma and hydrothermal system in Oman ophiolite and in IODP Hole 1256D: Fossilization of a dynamic melt lens at fast spreading ridges

Lyderic France, Benoit Ildefonse, Juergen Koepke

Geochemistry Geophysics Geosystems G3
AN ELECTRONIC JOURNAL OF THE EARTH SCIENCES
Published by AGU and the Geochemical Society

Article
Volume 10, Number 10
21 October 2009
Q10O19, doi:10.1029/2009GC002652
ISSN: 1525-2027

Interactions between magma and hydrothermal system in Oman ophiolite and in IODP Hole 1256D: Fossilization of a dynamic melt lens at fast spreading ridges

Lydéric France
Géosciences Montpellier, Université Montpellier 2, CNRS, CC60, F-34095 Montpellier CEDEX 5, France (lfrance@um2.fr)

Also at Institut für Mineralogie, Leibniz Universität Hannover, Callinstrasse 3, D-30167 Hannover, Germany

Benoit Ildefonse
Géosciences Montpellier, Université Montpellier 2, CNRS, CC60, F-34095 Montpellier CEDEX 5, France

Juergen Koepke
Institut für Mineralogie, Leibniz Universität Hannover, Callinstrasse 3, D-30167 Hannover, Germany

[1] The transition between the small melt lens observed on top of fast spreading ridge magma chambers and the overlying sheeted dike complex marks the interface between magma and the hydrothermal convective system. It is therefore critical to our understanding of fast spreading ridge accretion processes. We present maps of two areas of the Oman ophiolite where this transition zone is observed as continuous outcrops. Our observations, which include the base of the sheeted dike being crosscut by gabbros, are consistent with episodic dike injections in a steady state model but also suggest that the root of these dikes is commonly erased by vertical movements of the top of the melt lens. Dike assimilation is a possible mechanism for incorporating hydrated phases, which result from hydrothermal alteration, to the melt lens during upward migrations of its upper boundary. Upward migrations are also responsible for a granoblastic overprint of the root of the dikes that is also observed in the stoped diabase xenoliths. This granoblastic overprint attests to reheating of previously hydrothermally altered lithologies which can even trigger hydrous partial melting due to the lowering of the solidus of mafic lithologies by the presence of a water activity. Clinopyroxenes present in these granoblastic lithologies are typically low in Ti and Al content, thus strongly contrasting with corresponding magmatic clinopyroxene. This may attest to the recrystallization of clinopyroxenes after amphiboles under the peculiar conditions present at the root zone of the sheeted dike complex. Downward migrations of the top of the melt lens result in the crystallization of the isotropic gabbros at its roof, which represent the partly fossilized melt lens. Melt lens fossilization eventually occurs when magma supply is stopped or at the melt lens margins where the thermal conditions become cooler. Melt lens migration, recrystallization of hydrothermally altered sheeted dikes during reheating stages, and assimilation processes observed in the Oman ophiolite are consistent with the observations made in IODP Hole 1256D. We propose a general dynamic model in which the melt lens at fast spreading ridges undergoes upward and downward movements as a result of either eruption/replenishment stages or variations in the hydrothermal/magmatic fluxes.

Components: 34,517 words, 15 figures, 2 tables.

Keywords: fast spreading mid-ocean ridges; Oman ophiolite; hydrothermal system; melt lens; axial magma chamber; ODP.

Index Terms: 3614 Mineralogy and Petrology: Mid-oceanic ridge processes (1032, 8416); 3625 Mineralogy and Petrology: Petrography, microstructures, and textures; 3660 Mineralogy and Petrology: Metamorphic petrology.

Received 29 May 2009; **Revised** 25 August 2009; **Accepted** 2 September 2009; **Published** 21 October 2009.

France, L., B. Ildefonse, and J. Koepke (2009), Interactions between magma and hydrothermal system in Oman ophiolite and in IODP Hole 1256D: Fossilization of a dynamic melt lens at fast spreading ridges, *Geochem. Geophys. Geosyst.*, *10*, Q10O19, doi:10.1029/2009GC002652.

Theme: Formation and Evolution of Oceanic Crust Formed at Fast Spreading Rates
Guest Editors: D. A. H. Teagle and D. Wilson

1. Introduction

[2] The structure of fast spreading ridges is inferred from geophysical studies [e.g., *Morton and Sleep*, 1985; *Detrick et al.*, 1987; *Harding et al.*, 1989; *Kent et al.*, 1990] and from structural observations and mapping in ophiolites, in particular the Oman ophiolite [e.g., *Hopson et al.*, 1981; *Pallister and Hopson*, 1981; *Nicolas et al.*, 1988a, 2000; *Umino et al.*, 2003]. Geophysical studies have revealed the presence of a partly to totally molten melt lens (~30 to 100 m thick) at the top of the mostly crystallized magma chamber [e.g., *Sinton and Detrick*, 1992; *Hussenoeder et al.*, 1996; *Collier and Singh*, 1997; *Singh et al.*, 1998; *Dunn et al.*, 2000]. The composition and evolution of this thin melt lens play a key role in oceanic crust genesis as it feeds, at least partly, the upper and lower crust [e.g., *Sinton and Detrick*, 1992; *Boudier et al.*, 1996]. This horizon is also a major exchange interface between seawater and the oceanic crust as it is located at the root of the sheeted dike complex, where the hydrothermal convective system and the melt lens can meet and interact. Several descriptions of the gabbro/sheeted dike transition zone in ophiolites have been published, to attempt understanding the complex structural and petrological relationships within this zone [*Rothery*, 1983; *Nicolas and Boudier*, 1991; *MacLeod and Rothery*, 1992; *Gillis and Roberts*, 1999; *MacLeod and Yaouancq*, 2000; *Coogan et al.*, 2003; *Gillis*, 2008; *Nicolas et al.*, 2008].

[3] The IODP (Integrated Ocean Drilling Program) drilled Hole 1256D into a ~15 Ma crust that formed at the East Pacific Rise at a superfast spreading rate [*Teagle et al.*, 2006]. It is to date the only place in present-day oceanic crust where the uppermost gabbros below the sheeted dike complex has been sampled in situ below a continuous, intact section of upper oceanic crust [*Teagle et al.*, 2006; *Wilson et al.*, 2006; *Alt et al.*, 2007]. Studies in ophiolites or in present-day oceanic crust have led to the elaboration of a variety of models for the evolution of the complex magmatic/hydrothermal interface that constitutes the gabbro/sheeted dike transition zone. It is presented either as a steady state boundary layer [*Rothery*, 1983; *Nicolas and Boudier*, 1991; *MacLeod and Yaouancq*, 2000; *Nicolas et al.*, 2008], or as a dynamic one [*Gillis and Roberts*, 1999; *Coogan et al.*, 2003; *Wilson et al.*, 2006; *Gillis*, 2008; *Koepke et al.*, 2008]. The processes occurring in this transition zone, and the relationships between observed present-day lithologies and the melt lens at the time of accretion are still debated [e.g., *MacLeod and Yaouancq*, 2000; *Gillis*, 2008; *Nicolas et al.*, 2008].

[4] *Nicolas et al.* [2008] postulated that understanding the complex processes acting at the sheeted dike/gabbro transition requires studying undisturbed portions of the ridge, away from domains where accretion was under the influence of discontinuities due to ridge propagation or segmentation. In the present study, we have mapped in details the gabbro/sheeted dike transition zone in two localities of the Oman ophiolite that are, based on large-scale structural mapping [*Nicolas et al.*, 2000], away from major ridge axis tectonic activity. This study bears information on the evolution of the melt lens, and suggests a way to reconcile the apparently contrasting, previously published models.

2. Background

[5] At fast spreading ridges, the upper oceanic crust is composed of, from top to bottom, lavas, sheeted dikes, and isotropic ophitic gabbros (and associated coarse-grained gabbros and "oceanic plagiogranites"). The foliated gabbros, and layered gabbros form the lower crust. Many models, based on thermal modeling and/or ophiolite field data, have

been proposed for the formation of the igneous lower crust [e.g., *Sleep*, 1975; *Nicolas et al.*, 1988b; *Nicolas*, 1989; *Henstock et al.*, 1993; *Phipps Morgan and Chen*, 1993; *Quick and Denlinger*, 1993; *Nicolas and Boudier*, 1995; *Boudier et al.*, 1996; *Kelemen et al.*, 1997; *MacLeod and Yaouancq*, 2000; *Garrido et al.*, 2001]. Most recent models predict that the lower crust is fed from the top, through subsidence of the crystallized material from the melt lens, and/or from the bottom through sill injections [*Boudier et al.*, 1996; *Kelemen et al.*, 1997; *MacLeod and Yaouancq*, 2000; *Nicolas et al.*, 2009]. The balance between these two processes, however, remains poorly constrained and is still debated [e.g., *VanTongeren et al.*, 2008; *Webb*, 2008]. *MacLeod and Yaouancq* [2000] proposed that the lower crust is not fed from the axial melt lens, and that the foliated gabbros in the upper part of the igneous section only preserve the last increment of strain during crystallization in an upwelling melt flow. They observed that plagioclase zoning tends to increase up-section from the layered gabbros to the foliated gabbro, possibly reflecting the evolution of the melt as it migrates toward the top of the crystal mush pile. In contrast, other detailed studies of the high-level gabbros in the Oman ophiolite suggest that the melt lens does play a role in the genesis of the lower crust through subsidence processes [*Coogan et al.*, 2002; *Nicolas et al.*, 2009].

[6] The upper crust (volcanics and sheeted dike) is considered to be injected from the melt lens [e.g., *MacLeod and Yaouancq*, 2000]. However, it may not sample the whole melt lens. Based on observations made at Hess Deep (ODP Site 894), *Natland and Dick* [1996] proposed that the melt lens is partly filled with highly fractionated melts, too dense to erupt. These uneruptable melts are expelled from the underlying crystal mush column and seem to play a minor role in the upper crust accretion as they are expected to lie on the melt lens floor. The detailed structural, petrological, and geochemical study of the Wadi Abyad section, in the Oman ophiolite [*MacLeod and Yaouancq*, 2000] shows that, even if some highly fractionated pegmatitic gabbros may form up to 40% of the outcrops in some parts of the isotropic ophitic gabbro horizon, they are always subordinated to finer-grained and more magnesian gabbro. *MacLeod and Yaouancq* [2000] interpret the Fe-Ti pegmatitic gabbros as melts differentiated under reducing conditions and low water activities, at the border of the melt lens. They also propose that the average composition of the whole isotropic gabbro horizon represents the melt lens composition; their calculations lead to Mg # of 65 and a TiO_2 content of 1.1 wt %, which is relatively similar to the associated sheeted dikes and to typical N-MORB erupted at intermediate to fast spreading ridges [e.g., *Klein*, 2003].

[7] The evolution and stability of the melt lens, as well as its relationships with the overlying hydrothermally altered lithologies are also debated. These points are discussed through detailed studies of the root zone of the sheeted dike complex. This zone is composed of fine-grained isotropic ophitic gabbro, pegmatitic gabbro, some Fe-Ti gabbro and diorite, and oceanic plagiogranites. It has been described in the Oman ophiolite [*Rothery*, 1983; *Nicolas and Boudier*, 1991] and recently revisited in details [*Nicolas et al.*, 2008]. Based on petrological and structural observations, *Nicolas et al.* [2008] present a new steady state model for the evolution of the melt lens. They propose that most of the isotropic gabbro horizon, called "root zone of the sheeted dike complex," is generated by hydrous partial melting triggered by the intrusion of hydrothermal fluids in the recently crystallized, still hot, base of the sheeted dike complex. In this model, the root zone lithologies do not represent the crystallization of the melt lens, which is assumed to pinch out at its tips. *Macleod and Yaouancq* [2000] also describe the root zone of the sheeted dike complex in the Oman ophiolite as a steady state horizon, but in contrast with *Nicolas and Boudier* [1991] and *Nicolas et al.* [2008], they interpret it as the crystallized melt lens under anhydrous and reducing conditions, implying little assimilation of hydrated doleritic roof material. However, they show some assimilation evidences [*MacLeod and Yaouancq*, 2000, Figure 2d]. Reheating and assimilation in the root zone are documented in the Oman ophiolite [*Coogan et al.*, 2003; *Gillis*, 2008], in the Troodos ophiolite [*Gillis and Roberts*, 1999; *Gillis*, 2002; *Gillis and Coogan*, 2002; *Gillis*, 2008], and at Pito Deep and Hess Deep [*Gillis*, 2008]. *Wilson et al.* [2006] and *Koepke et al.* [2008] recently described assimilation and reheating features within the root zone of the sheeted dike complex in the IODP Hole 1256D, the first and so far only borehole in present-day intact ocean crust that reaches the contact between sheeted dikes and gabbro. *Nicolas et al.* [2008] discuss these results by pointing out that reheating and assimilation features are well known in the Oman ophiolite in areas affected by ridge segmentation [*Juteau et al.*, 1988; *MacLeod and Rothery*, 1992; *Nicolas and Boudier*, 1995; *Boudier et al.*, 2000; *Adachi and Miyashita*, 2003; *Miyashita et al.*, 2003; *Umino et al.*, 2003], but have not been

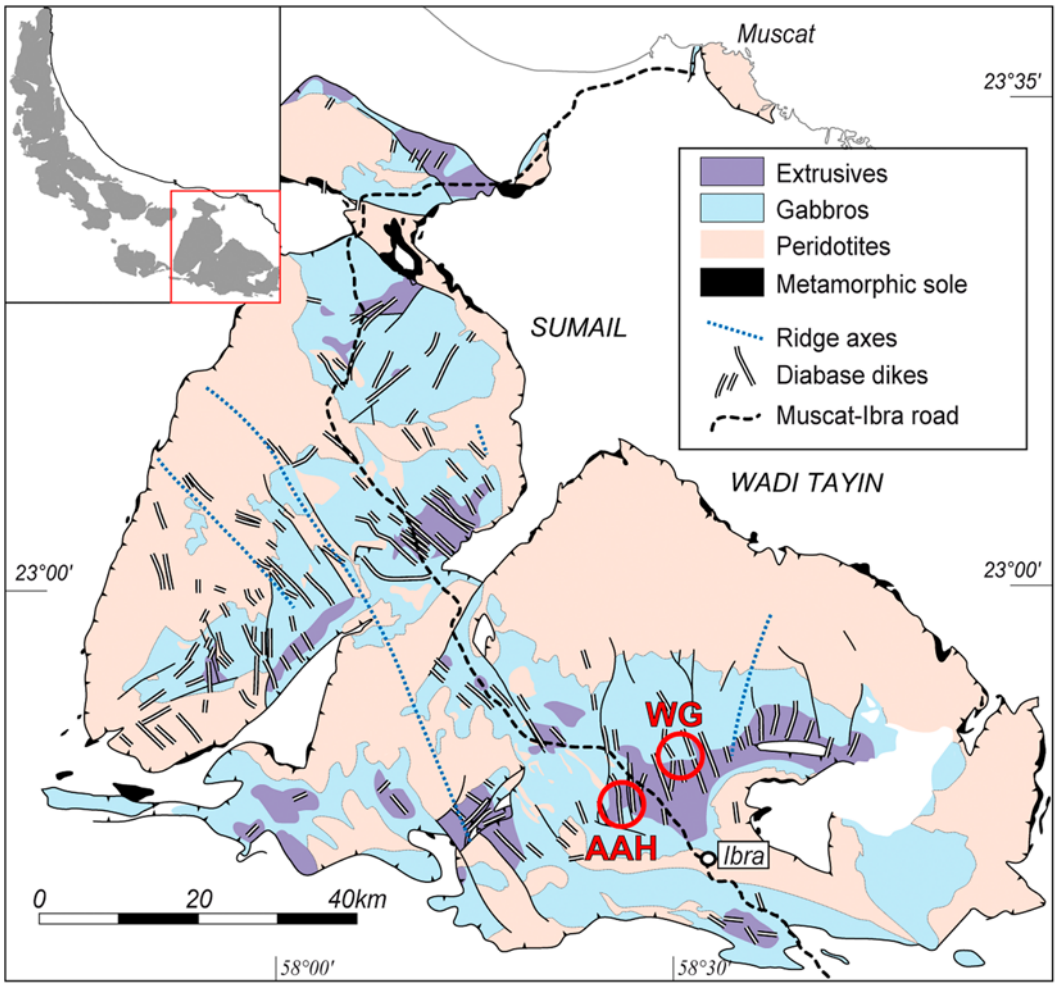

Figure 1. Simplified geological and structural map of the southern massifs and location (red box) in the Oman ophiolite [after *Nicolas et al.*, 2000]. Red circles indicate the locations of the studied zones (WG, Wadi Gideah; AAH, Al Ahamadi Hills).

described in "undisturbed" zones, away from discontinuities, yet. They suggest that reheating and assimilation, in the Oman and Troodos ophiolite, and in the IODP borehole could be related to ridge segmentation.

[8] To further constrain the characteristics of the transition from gabbros to the sheeted dike complex (i.e., the interface between the magmatic and the hydrothermal systems), we have mapped in details this transition in two "undisturbed" areas of the Oman ophiolite (Wadi Gideah area, in the Wadi Tayin Massif, and Al Ahmadi Hills area, in the Ibra plain at the southern end of the Wadi Tayin Massif). Because of its lithological heterogeneity, and of the presence of many igneous contacts and fractures, the root zone of the sheeted dike complex is a zone of preferential meteoric alteration and outcrops very poorly (see, e.g., *MacLeod and Yaouancq* [2000, Figure 1], which shows the outcrops discontinuity). Observations from these two regions are made over continuous outcrops and are consistent with many other visited sites where outcrops are not continuous.

3. Field Observations

[9] The two studied areas are located in the well-exposed Wadi Tayin Massif, one of the southern Massifs in the Oman ophiolite where ridge segmentation effects are minor [*Nicolas et al.*, 2000] (Figure 1). The southern massifs are large and flat-bottomed synclines with the sheeted dike and subvertical gabbro foliation trending ~NW–SE. The NW–SE segments are opened in an older domain where the sheeted dike trends ~NE–SW. The Wadi Gideah area is situated in the Jebel Dimh, 10 km to the north of Ibra and ~10 km to the east of the main road

between Muscat and Ibra. The Al Ahmadi Hills are located in the large Wadi Nam, 6 km to the NW of the Al Ahmadi village and 10 km to the NNW of the town of Ibra.

3.1. Wadi Gideah Area

[10] The mapped area in Wadi Gideah extends from the foliated gabbro in the north to the sheeted dikes in the south, and includes in between the heterogeneous, isotropic ophitic gabbro horizon (Figure 2a). The foliated gabbros present the same characteristics as anywhere else in the Oman ophiolite; they are granular, and display a subvertical foliation trending N–S (Figure 3). Close to the contact with the foliated gabbros, the isotropic ophitic gabbro horizon is very heterogeneous; it is composed of coarse-grained lithologies such as hornblende-olivine-gabbro or hornblende-gabbro, which contain some strongly altered xenoliths of predominantly fine-grained recrystallized diabase, but also gabbro and hornblende-diorite. The relationships between the different lithologies in this particular place are unclear because of the intense weathering. To the south, up-section, isotropic ophitic gabbros become more homogeneous. Some isolated narrow and elongated meter sized zones display a foliation (~N–S, subvertical) that seems to underline the contacts with gabbro injections. Rounded xenoliths of gabbro and diabase, about 10 × 10 cm on average, are accumulated at small hill summits in the whole isotropic gabbro horizon (Figures 2 and 4a). Magmatic breccias with a leucocratic matrix enclosing gabbro or dike xenoliths are also observed (Figures 2 and 4b). Except for one occurrence close to the foliated gabbro (Figure 2), these breccias are located close to, or at the contact between the isotropic ophitic gabbro horizon and the sheeted dikes. Figures 2b and 2c show two hills in the ophitic gabbros topped by sheeted dike. No fault is observed between these two hills. The vertical offset of the contact between gabbros and sheeted dike is consequently assumed to represent initial depth variations of this contact along the ridge axis. To the south, the sheeted dikes present the same characteristics as anywhere else in the Oman ophiolite, and trend N–S, subvertical (Figure 3). Each dike is about 1 to 1.5 m wide and present chilled margins against other dikes. Some later dikes with chilled margins, also 1 to 1.5 m wide, crosscut the isotropic gabbros and the previous sheeted dikes; they are subparallel to the sheeted dike complex (Figure 5).

[11] Isotropic ophitic gabbros intrude the base of the sheeted dikes, and locally assimilate dike fragments (Figure 6). Sparse diabase xenoliths are locally observed. Gabbros clearly crosscut former chilled margins (Figure 6), and locally intrude the sheeted dike base, but do not invade it further than about 1 m above the main contact. Some contact outcrops show a gradation toward the contact from gabbroic rocks to more leucocratic ones (Figures 6c and 6e). Coarse-grained isotropic ophitic gabbros are also common in the root zone and at the contact with xenoliths (Figure 6f).

[12] Dikes truncated by ophitic gabbro show well-equilibrated (with ~120° triple junctions), fine-grained granular textures, called hereafter "granoblastic textures" (Figure 7a). These textures are clearly distinct from the doleritic textures classically observed in Oman ophiolite sheeted dikes. Recrystallized texture is observed on both sides of dike margins; that is, it overprints both last and former dikes (Figures 7a and 7b). The average grain size in the granoblastic margins overprinting the chilled margins is ~10 μm. Ten centimeters away from the margins, the recrystallized textures display coarser granular grains (~50 μm; Figure 7b); plagioclases are largely less recrystallized than pyroxenes. Patches with granoblastic texture (0.5 to 1 mm wide) are also observed in the uppermost isotropic gabbros (Figure 7c). The paragenesis of granoblastic domains includes plagioclase, clinopyroxene, amphibole, magnetite, and ilmenite. Granoblastic texture lithologies are particularly rich in oxides (Figures 7a, 7b, 7e, and 7g). The corresponding mineral assemblages are commonly complex with different generations of clinopyroxenes and amphiboles (Figure 7f) and clinopyroxenes commonly contain numerous tiny oxide inclusions. Oxide inclusion-rich clinopyroxene veins (100 to 200 μm wide) in the base of the sheeted dikes are crosscut by intrusive gabbros (Figures 7g and 7h). The leucocratic lithologies (oceanic plagiogranites) that are sometimes present at the base of the dikes contain tiny clinopyroxenes (20 to 50 μm) associated with oxides, suggesting that these correspond to relics of parageneses from the granoblastic stage. These minerals have rounded shapes and appear to be relics of former larger grains. This observation is critical to constrain the origin (differentiation versus hydrous partial melting) of these oceanic plagiogranites (see discussion below). All samples are moderately to strongly altered in the greenschist facies; actinolite and albitized plagioclases replace magmatic ones, clinopyroxenes and higher-temperature amphibole (hornblende and pargasite). In some samples the granoblastic texture is so strongly altered that it is hardly recognizable (Figure 7d).

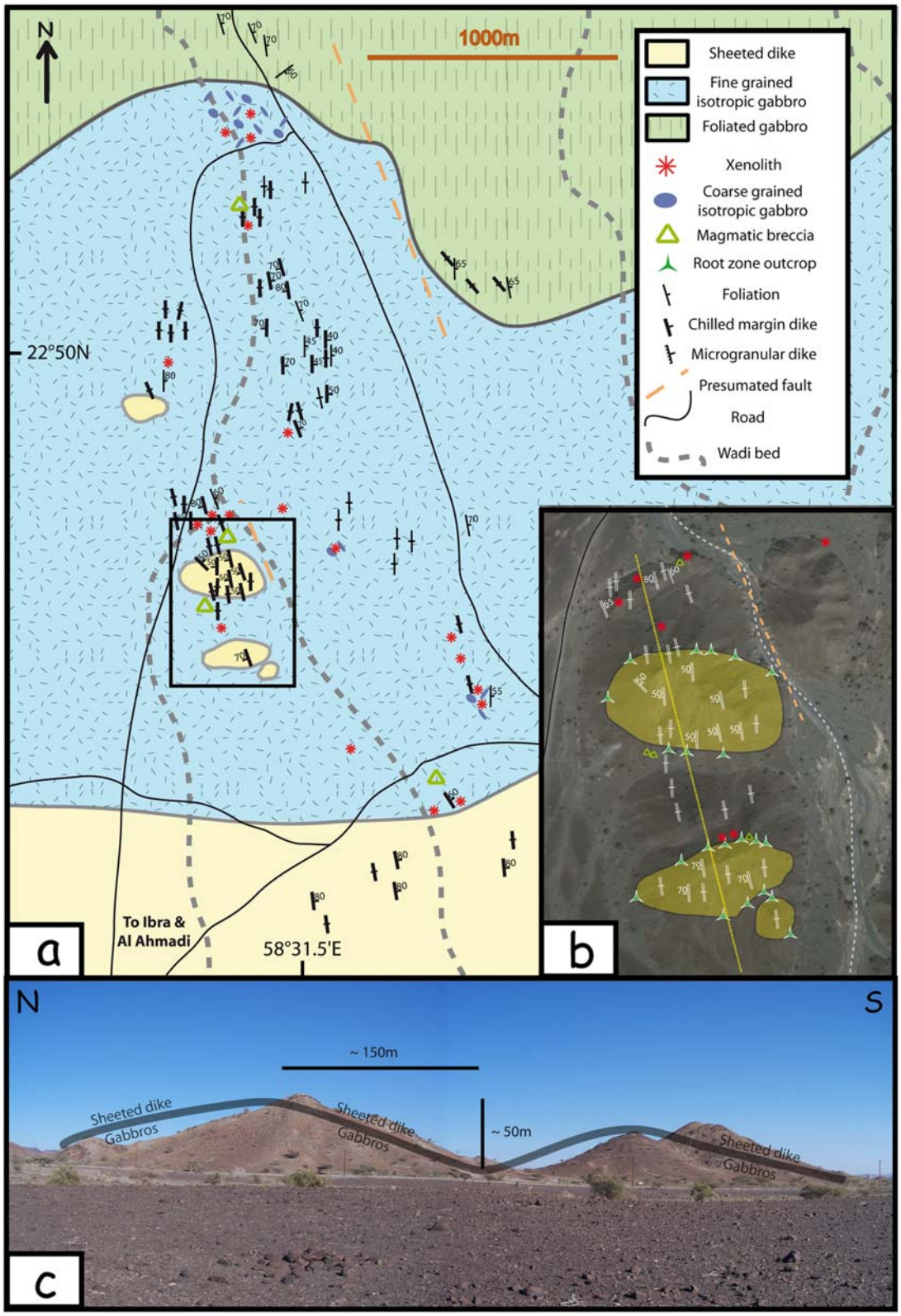

Figure 2. Wadi Gideah area. (a) Geological and structural map. The black rectangle represents the location of Figure 2b. (b) Zoom on the two hills that have their summits and southern flanks composed of sheeted dikes and their northern flanks composed of gabbros. The yellow line indicates the position of the cross section in Figure 2c. (c) Cross section showing the two hills from Figure 2b. The thick gray line indicates the gabbro/sheeted dike transition that is precisely mapped in Figure 2b. No fault has been observed.

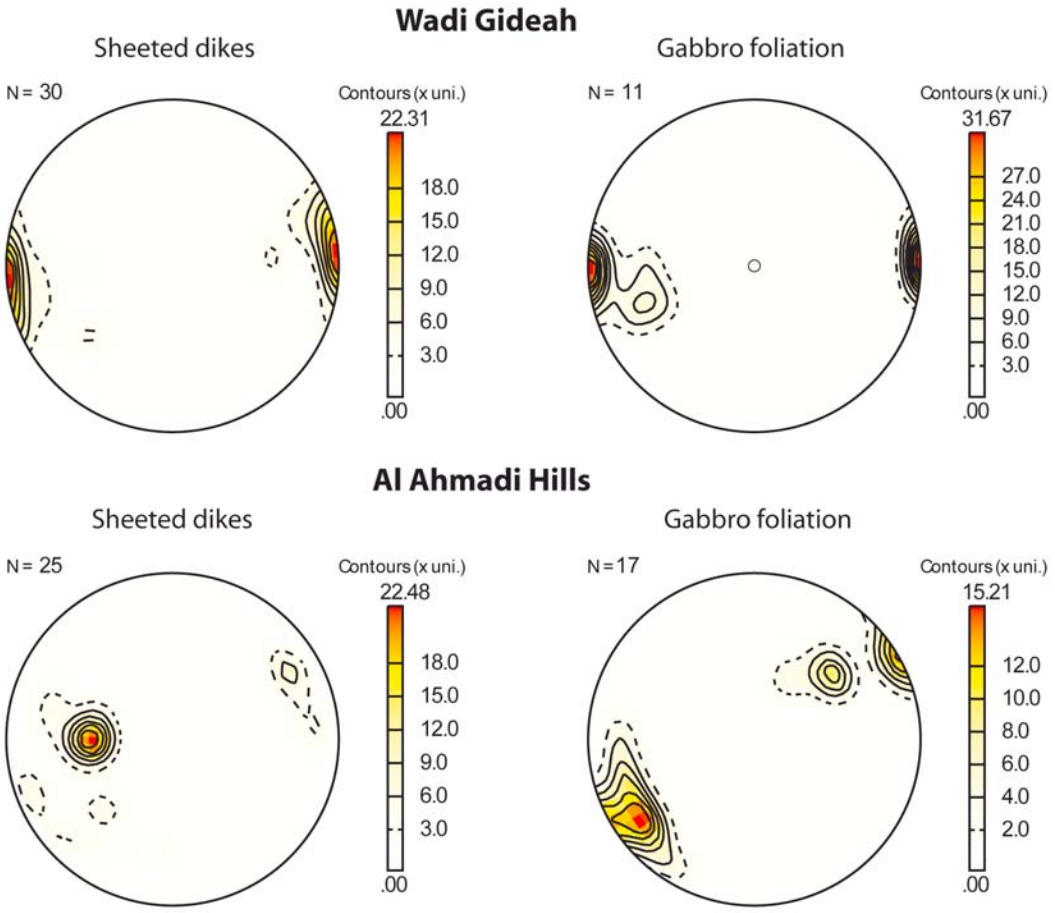

Figure 3. Stereonets (lower hemisphere, nonpolar data, geographical reference system) showing field structural measurements: (left) sheeted dike and (right) magmatic foliations in foliated gabbros (top) in the Wadi Gideah area and (bottom) in the Al Ahmadi Hills area.

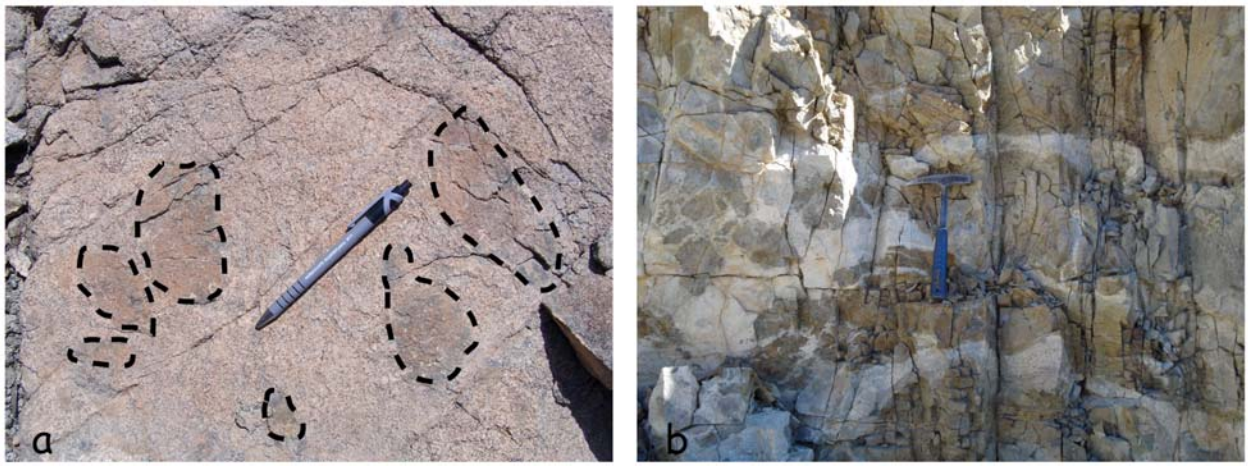

Figure 4. (a) Xenoliths of granoblastic dikes in isotropic ophitic gabbro and (b) magmatic breccia consisting of recrystallized sheeted dike within a silicic (oceanic plagiogranite) matrix. Both outcrops are in the Wadi Gideah area.

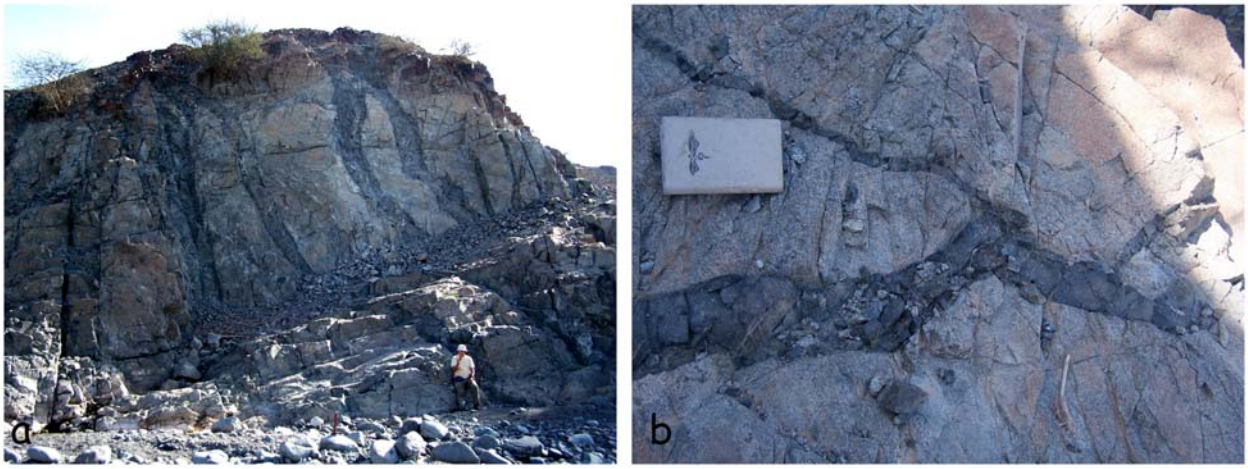

Figure 5. Late diabase dikes crosscutting isotropic ophitic gabbros in the Wadi Gideah area.

3.2. Al Ahmadi Hills

[13] The Al Ahmadi Hills are aligned along a small, 3000 m long and ~50 m high ridge that trends NW–SE (Figure 8a). At the northern tip of this ridge, the first lithology encountered is olivine gabbro, with a steep, strong magmatic foliation oriented 160E75 on average (Figures 3 and 9a). In some rare, about 1 to 5 m large domains, the foliation is hardly identifiable in the field. Microscopic observations show that the foliation is similar to what is observed in the other foliated samples, with olivine mantled by orthopyroxene and pargasite (Figure 9b). This assemblage is described by *Koepke et al.* [2005a, 2005b] and *Nicolas et al.* [2003], and may trace late magmatic processes such as hydrous partial melting reactions or late crystallization in the presence of water.

[14] The transition to the next horizon above, mostly composed of isotropic ophitic gabbros, is sharp. It occurs over less than 10 m. This horizon is strongly altered in the greenschist facies, as shown by the abundance of actinolite. Immediately above this contact, the ophitic gabbros contain numerous large xenoliths (up to 1.5 m large; Figures 8a, 8b, and 8d), which are composed either of oxide-rich granoblastic overprinted dikes (Figure 9c) or of gabbroic rocks. This area is composed of about 60% isotropic ophitic gabbros, 30% xenoliths, and nearly 10% pegmatitic gabbros very similar to those of Wadi Gideah (Figures 6d and 6f), forming the matrix around the xenoliths. In some localized (~10 m) zones, xenoliths represent up to 90% of the outcropping material. Xenolith accumulation appears more abundant in the lower third of the isotropic ophitic gabbro section (Figures 8a and 8d). Xenoliths and pegmatitic gabbros become less abundant, and nearly disappear up-section, to finally reappear close to the contact with the sheeted dikes.

[15] As observed in Wadi Gideah (Figure 6), the contact between the isotropic ophitic gabbros and the overlying sheeted dike complex is very sharp. Gabbros are again intrusive in the sheeted dike and crosscut former dike margins. Close to this contact, dike xenoliths are locally accumulated, generally small (~10 cm, Figure 8c), and form ~1 m wide clusters (Figures 8c and 8d). These xenoliths have granoblastic textures; they are totally metamorphosed in the greenschist facies and the granoblastic texture is commonly blurred. The base of the dikes is also very altered but the recrystallized granular texture, associated to an enrichment in granular oxides, is still recognizable in some samples (Figure 9d); these are interpreted as relics, after subsequent alteration, of the granoblastic overprint. Because of the strong greenschist facies overprint and of the strong weathering, it is not possible to estimate the vertical extent of the granoblastic overprint. These textures are identical to those observed in the same structural position in the Wadi Gideah area.

[16] Up-section, the Al Ahmadi hills continue over ~1000 m with the sheeted dike complex, oriented 0E50 on average (Figure 3). The sheeted dikes are typical of what is observed elsewhere in the Oman ophiolite; it is made of parallel, about 1 to 1.5 m wide, greenschist altered dikes, bounded by dark chilled margins against other dikes.

[17] In the whole section, late dikes crosscut other lithologies. In the lower part of the section, late dikes display microgranular margins that are nearly free of oxides (Figure 9e), and ophitic coarser grained center (Figure 9f). They grade up-section, close to

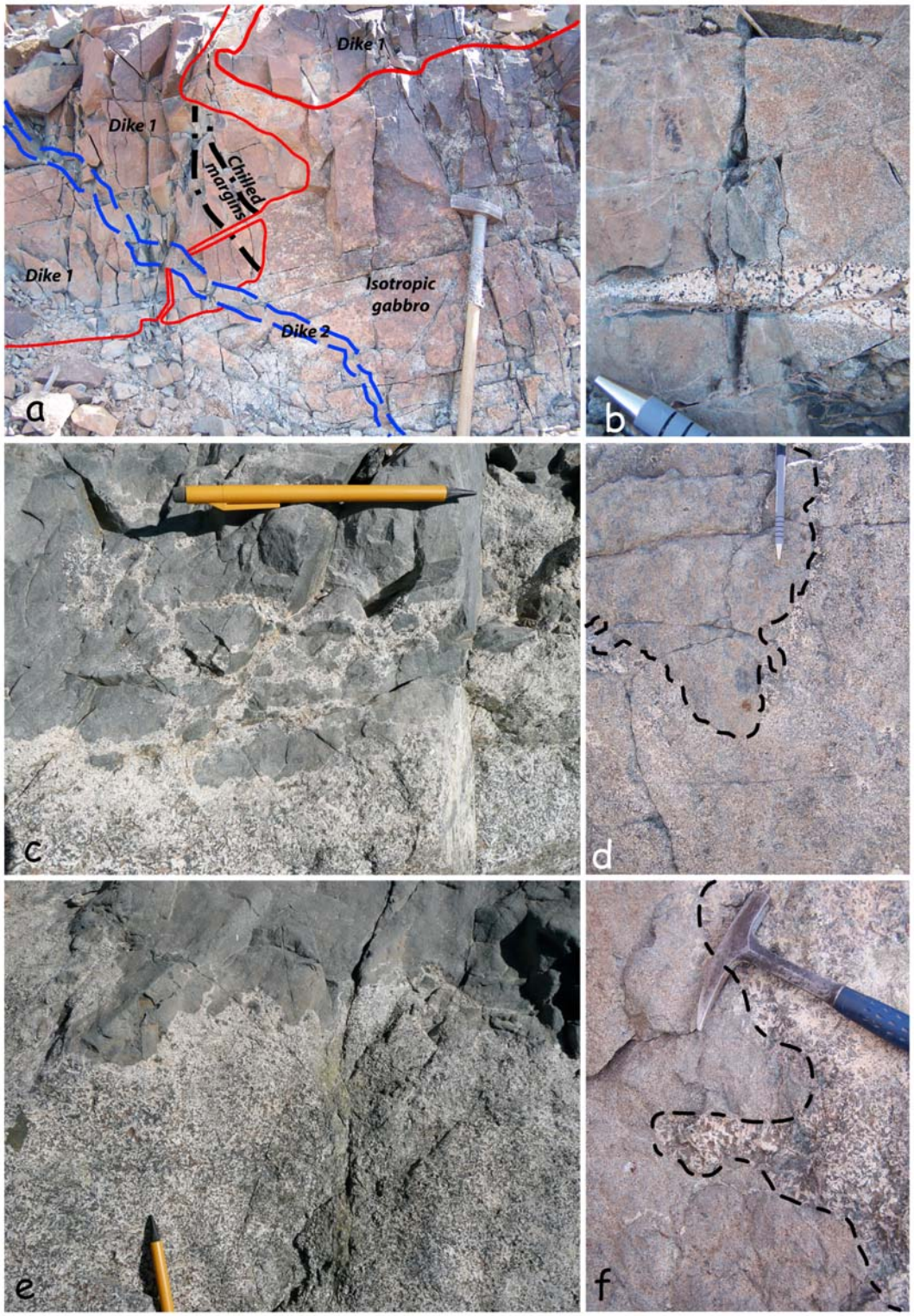

Figure 6. Outcrops in the root zone of the sheeted dikes. (a) Recrystallized sheeted dike (granoblastic dike) intruded by gabbro. Recrystallized chilled margins are crosscut by the intrusive gabbro. A late dike ("dike 2") crosscuts the gabbro and recrystallized dikes ("dike 1"). (b) Dioritic intrusion that crosscuts a recrystallized dike margin with granoblastic texture. (c and e) Gabbro assimilating recrystallized sheeted dike. The gradation to more leucocratic lithology at the contact is visible. A small shear zone affecting the dikes and gabbro is visible on the right side of Figure 106c. (d and f) Xenoliths of recrystallized dikes showing granoblastic texture in isotropic gabbro. Patches of coarser grained gabbro are observed around the xenolith in d), and all surrounding gabbro is pegmatitic in Figure 6f.

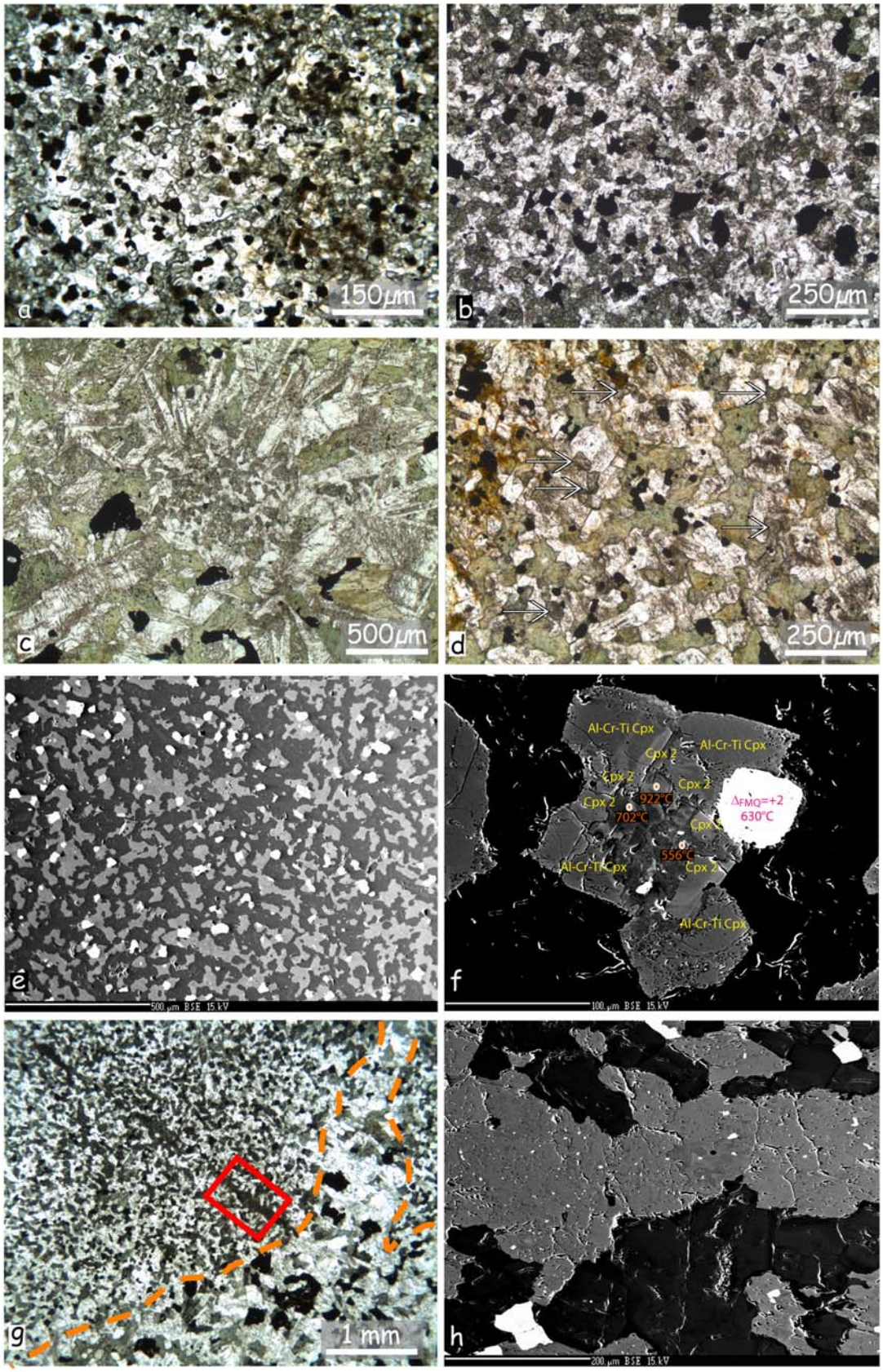
a
150μm
b
250μm
c
500μm
d
250μm
e
f
Al-Cr-Ti Cpx
Cpx 2
922°C
702°C
ΔFMQ=+2
630°C
556°C
g
1 mm
h

Figure 7

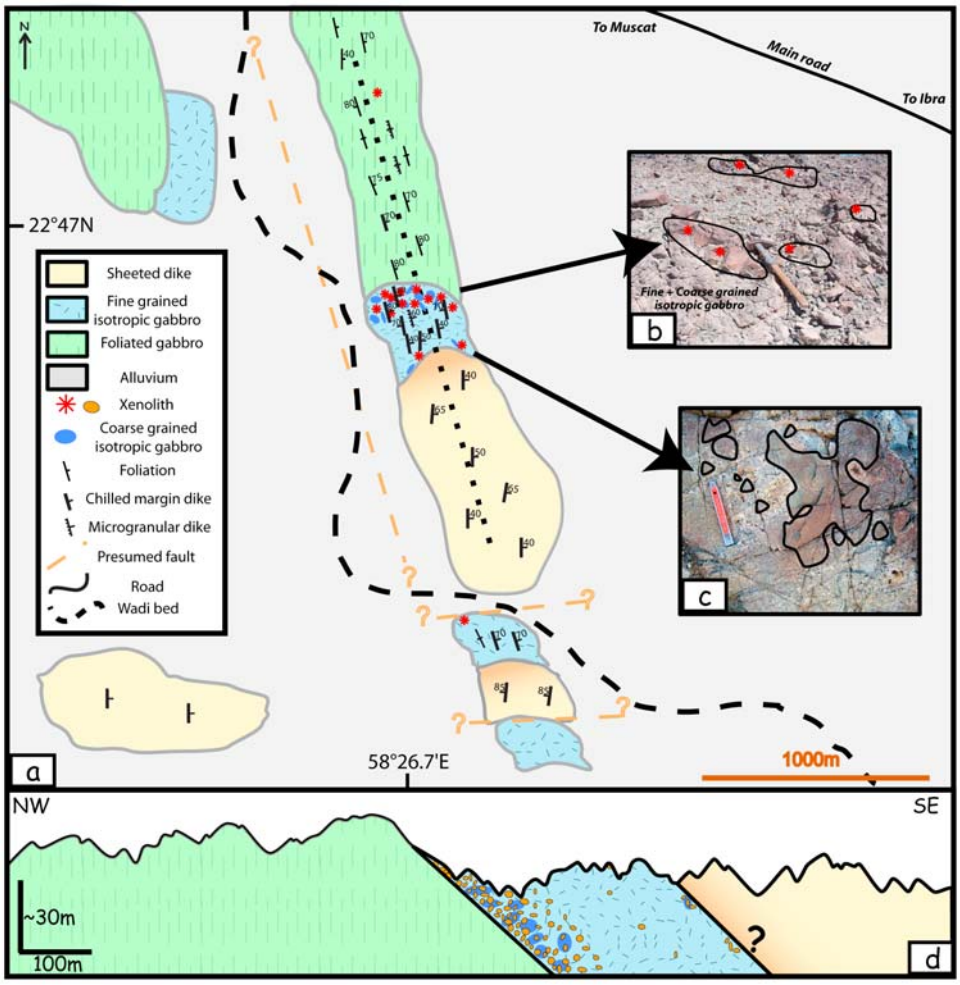

Figure 8. Al Ahmadi Hills area. (a) Geological and structural map. The dotted line indicates the location of the cross section in Figure 8d. (b) Large xenoliths of recrystallized dike fragments close to the foliated gabbro/isotropic gabbro transition. (c) Decimeter-sized xenoliths of recrystallized dikes close to the transition between isotropic gabbro and recrystallized sheeted dikes. (d) NW–SE cross section. Vertical exaggeration is ×3; the isotropic gabbro horizon is ~100 m thick. The base of the sheeted dike is reheated and recrystallized over a distance that is not constrained because of the strong weathering.

Figure 7. Photomicrographs and BSE images of samples from the Wadi Gideah area. (a) Fine-grained granoblastic texture with a high oxide concentration in a recrystallized dike margin (plane-polarized light). (b) Coarser-grained recrystallized texture in the center of a recrystallized dike (plane-polarized light). (c) Granoblastic patch in isotropic gabbro in the center of the picture (plane-polarized light). (d) Coarse-grained recrystallized texture partially erased by a strong greenschist facies alteration in a granoblastic dike (plane-polarized light). Arrows indicate granular grains. (e) BSE image of the granoblastic texture in a recrystallized dike. Dark gray minerals are plagioclases, light gray minerals are clinopyroxene + amphibole, and white minerals are oxides. (f) BSE image focusing on Fe-Mg minerals present in the granoblastic dikes. Different generations of clinopyroxenes (Cpx) and amphiboles are present (orange numbers indicate temperatures estimated with *Ernst and Liu* [1998]). The white phase is a mixture of ilmenite and magnetite. Redox and temperature estimates are calculated using *Sauerzapf et al.* [2008]. (g) Isotropic gabbro cross-cutting a recrystallized granoblastic dike. In the recrystallized dike, the truncated clinopyroxene vein is believed to derivate from a former amphibole bearing hydrothermal vein (cross-polarized light). The red square indicates the position of the BSE in Figure 7h. (h) BSE image of the truncated clinopyroxene vein in Figure 7g. Note the occurrence of numerous tiny oxide inclusions in the clinopyroxenes.

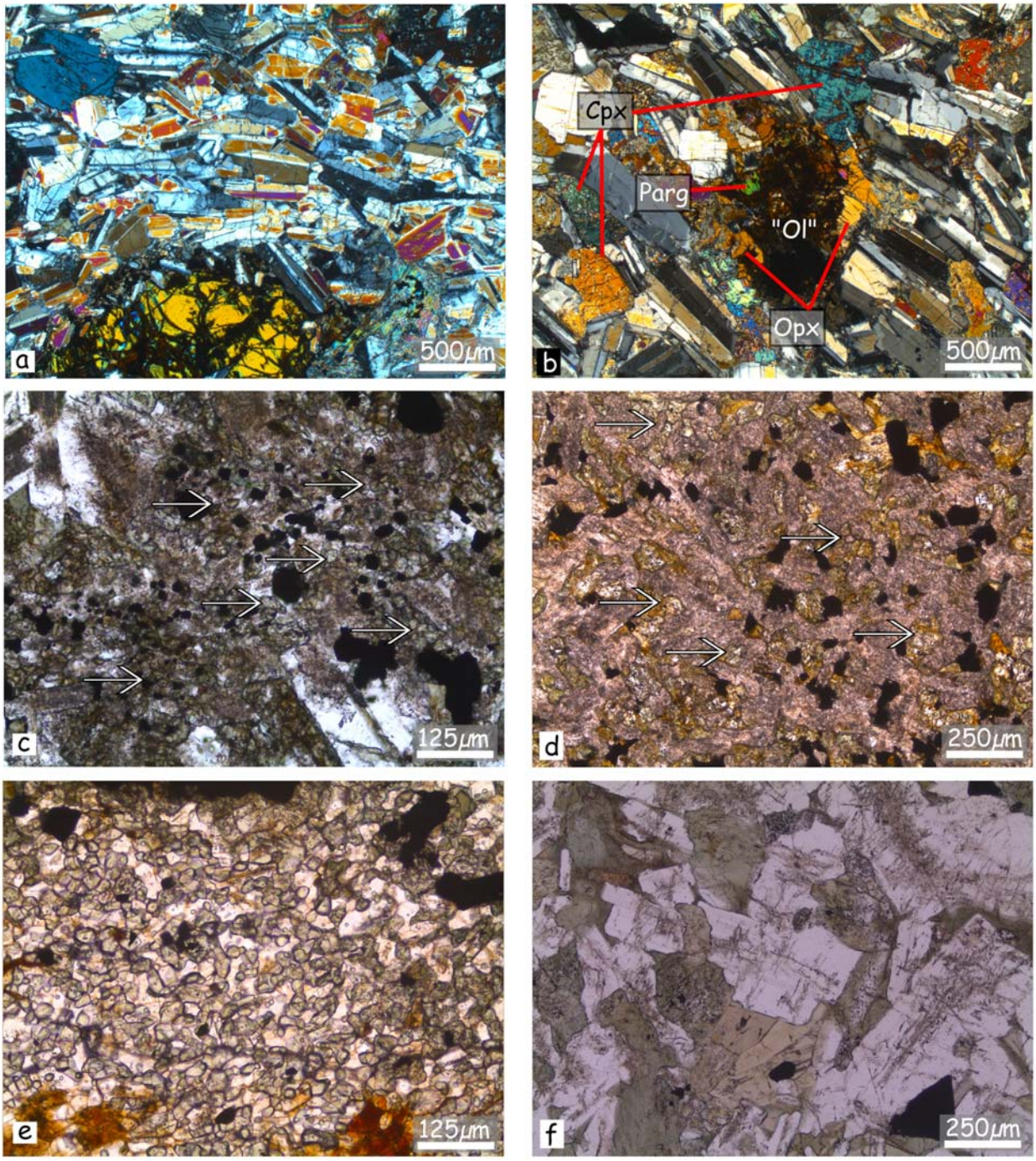

Figure 9. Photomicrographs of samples from the Al Ahmadi Hills area. (a) Foliated olivine-gabbro (cross-polarized light). (b) Altered olivine (Ol) surrounded by orthopyroxene (Opx) and pargasite (Parg) in the foliated gabbro domains where the foliation is hardly identifiable in the field (cross-polarized light). (c) Granoblastic overprint in a diabase xenolith. Arrows indicate the small granoblastic grains (plane-polarized light). (d) Strongly altered coarser-grained recrystallized texture from the base of the sheeted dike complex (center of a recrystallized dike: plane-polarized light). Arrows indicate granular grains. (e) Microgranular texture of a protodike margin (plane-polarized light). (f) Protodike center showing a texture similar to the isotropic ophitic gabbro (plane-polarized light).

the contact with the sheeted dikes, to diabase dikes with chilled margins. *Nicolas and Boudier* [1991] and *Nicolas et al.* [2008] described in the root zone of the sheeted dike complex similar dikes with ophitic texture in the center and microgranular margins, which they name "protodikes," and ascribed to slow cooling in a hot and hydrous environment. The magmatic protodikes depart from the metamorphic granoblastic truncated dikes in that only their margins display microgranular textures (e.g., compare Figure 7a with Figure 9e for the margins and Figure 7b with Figure 9f for the center of dikes). We interpret the late dikes observed in the mapped areas as protodikes that intrude the still hot, recently crystallized gabbros. Because a single protodike cannot be followed in the field over hundreds of meters, the textural transition from protodikes with microgranular margins to dikes with chilled margins up-section is not precisely located.

4. IODP Hole 1256D

[18] IODP Hole 1256D reached for the first time the sheeted dikes/gabbro transition in ultrafast spread oceanic crust [*Teagle et al.*, 2006; *Wilson et al.*, 2006; *Alt et al.*, 2007]. The sheeted dikes/gabbro transition is sharp and represents an intrusive contact similar to those observed in Oman (*Wilson et al.* [2006, Figure 4c] and Figure 6 herein). The base of the sheeted dike complex comprises recrystallized, granoblastic texture domains (granulitic facies) over ~60 m; this texture is identical to the granoblastic one described herein in samples from Oman (see for example the concordance between Figures 7a and 10a for the fine granoblastic lithologies and 7b and 10b for coarser-grained recrystallized ones). The section below the sheeted dike/gabbro contact has been resampled for this study (Table A1).

[19] *Wilson et al.* [2006] describe two granoblastic intervals that are interpreted as "screens of granoblastic dikes," the first one (~15 to 25 m thick) is located between two gabbroic bodies ("gabbro 1" (~45 m) and deeper "gabbro 2" (~15 m)) and the second one (very poorly recovered) at the bottom of the "gabbro 2" interval, close to the bottom of Hole 1256D. The first thick "screen of granoblastic dikes" (Figure 10c) is poorly recovered (<30%; Figure 11). However, even in the most continuous cores of this interval, granoblastic lithologies are crosscut by thin intrusions of gabbros and oceanic plagiogranites, with diffuse to sharp contacts (Figure 11).

[20] We have also observed in the core the presence of sparse, small (cm to ~10 cm) xenoliths in the upper part of the "gabbro 1" interval, at the contact with the base of the granoblastic dikes and, as described by *Wilson et al.* [2006], higher concentrations of xenoliths deeper in the "gabbro 2" interval, close to the bottom of the drilling hole. The sampled xenoliths show recrystallized textures similar to the ones of the base of the granoblastic dikes and to the ones of the thick "screen of granoblastic dikes" located between the "gabbro 1" and "gabbro 2" intervals. Granoblastic patches similar to those observed in Wadi Gideah (Figure 7c) are also observed in the "gabbro 1" and "gabbro 2" intervals (Figure 10d).

5. Mineral Compositions and Thermometry

[21] Mineral electron microprobe analyses were performed at Géosciences Montpellier and at the Institut für Mineralogie, Hannover using a Cameca SX 100 electron microprobe equipped with 5 spectrometers and an operating system "Peak sight." Data were obtained using a 15 KV acceleration potential, a static (fixed) beam, Kα emission from all elements, and the "PAP" matrix correction [*Pouchou and Pichoir*, 1991] in Hannover and its modification [*Merlet*, 1994] in Montpellier. Most element concentrations were obtained with a beam current of 15 nA and a counting time of 10 to 120 s on peak and background.

[22] Analyses presented herein (Table A1) were acquired on samples from the base of the Oman sheeted dike (granoblastic domains), from diabase xenoliths that are present in the isotropic ophitic gabbros, from coarse-grained gabbros that surround these xenoliths, from oceanic plagiogranites sampled at the base of the sheeted dikes, from a protodike, and from foliated gabbros. All Oman samples come from the Al Ahmadi Hills and Wadi Gideah areas. We also present for comparison analyses of IODP Hole 1256D samples. These samples come from the lowermost granoblastic dikes (just above the first recovered gabbro), from the "screen of granoblastic dikes" located between the "gabbro 1" and "gabbro 2" intervals, and from granoblastic xenoliths in gabbros.

5.1. Root Zone Lithologies and Protodikes

[23] In Oman samples, plagioclase compositions are very variable; they range from An_{10} to An_{57} in

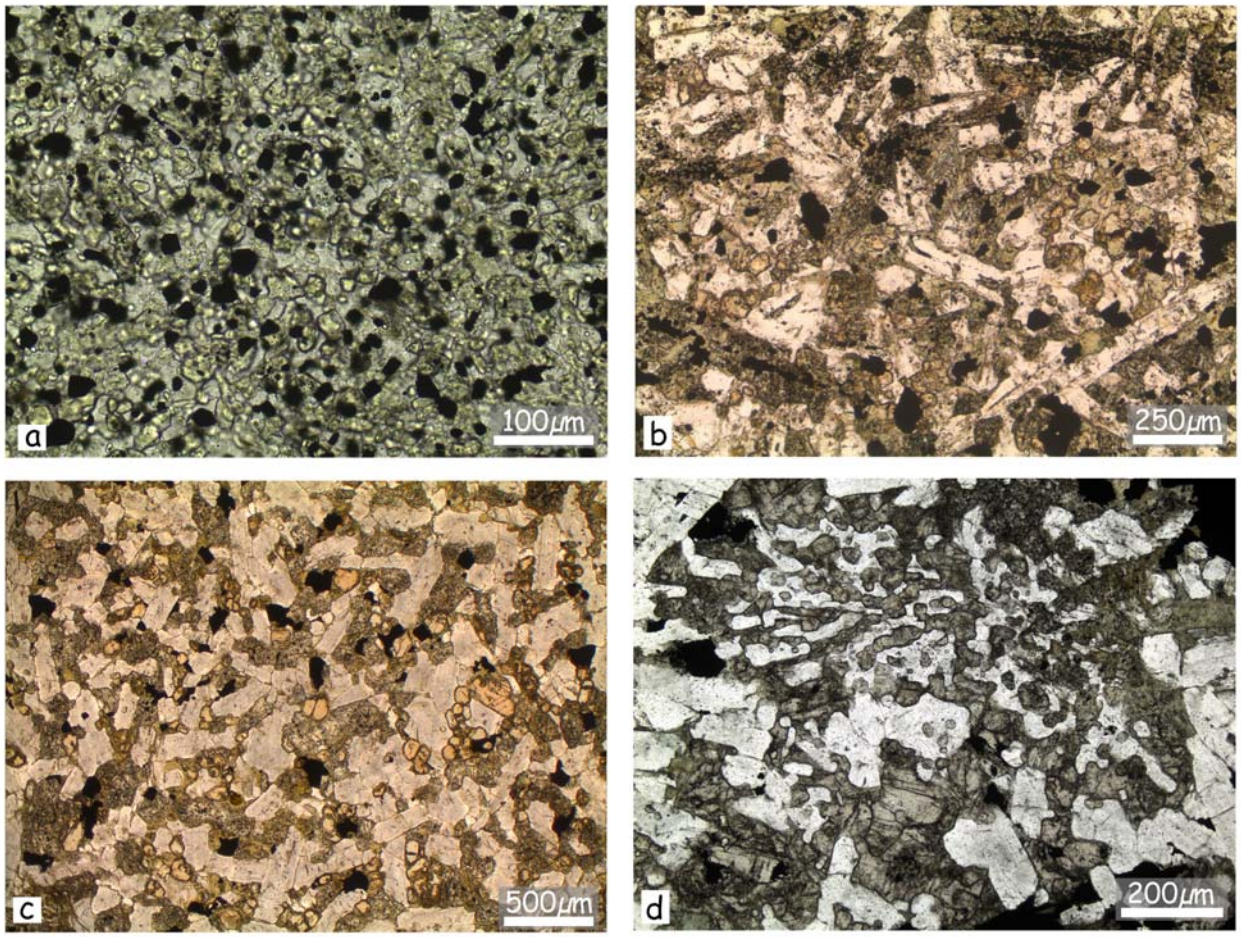

Figure 10. Photomicrographs of samples from IODP Hole 1256D (plane-polarized light). Photographs in Figures 10a and 10d are from the IODP database (Expedition 312; http://iodp.tamu.edu/janusweb/imaging/tsmicro.shtml). (a) High oxide concentration in a fine-grained granoblastic dike (recrystallized base of the sheeted dike complex; sample 312_1256D_205R1_10-14). (b) Coarser-grained, partially recrystallized texture (pyroxenes are granular and recrystallized) in diabase at the base of the granoblastic dike interval (sample 312_1256D_209R1_170-19). (c) Coarser-grained, partially recrystallized texture in the "granoblastic screen" located between gabbro 1 and gabbro 2 (interpreted as xenoliths of recrystallized dikes in the present study (see section 6.3 for further discussion); sample 312_1256D_227R1_30-34). Pyroxenes are granular, and oxide-bearing clinopyroxenes are inferred to crystallize after former amphiboles. (d) Patch with structure interpreted as a former granoblastic domain in isotropic gabbro (sample 312_1256D_223R3_1-6).

granoblastic lithologies and xenoliths, and reach An_{74} in the protodike (Figure 12). Clinopyroxene Mg # ranges from 59 to 72 in granoblastic lithologies and reaches 75 in the protodike (Figure 12). Al_2O_3 and TiO_2 are significantly low compared to typically magmatic clinopyroxenes from oceanic mafic rocks and to those obtained experimentally in corresponding tholeiitic systems (Figure 13). TiO_2 is strongly correlated with Al_2O_3 (with $Al_2O_3/TiO_2 \approx 3$) and shows an apparent linear trend pronounced at low concentrations (Figure 13). CaO contents are high, and Cr_2O_3 is nearly always under detection limits. Orthopyroxenes are present only in protodikes and have an Mg # of 68. Amphibole compositions are variables, including actinolite, hornblende, edenite, and pargasite. One granoblastic dike sample from the Wadi Gideah area contains zoned plagioclases, with An_{22} cores and An_{38} rims. Granoblastic patches observed in the isotropic ophitic gabbros (Figure 7c) are similar in compositions to other granoblastic lithologies, with An_{48} plagioclases and Mg # = 69 for clinopyroxenes. Oxide bearing clinopyroxene from the truncated veins observed at the sheeted dike/gabbro transition (Figures 7g and 7h) plot in the TiO_2 versus Al_2O_3 linear trend (Figure 13).

[24] In oceanic plagiogranites, plagioclases are albite to oligoclase with An ranging from 7 to 27.

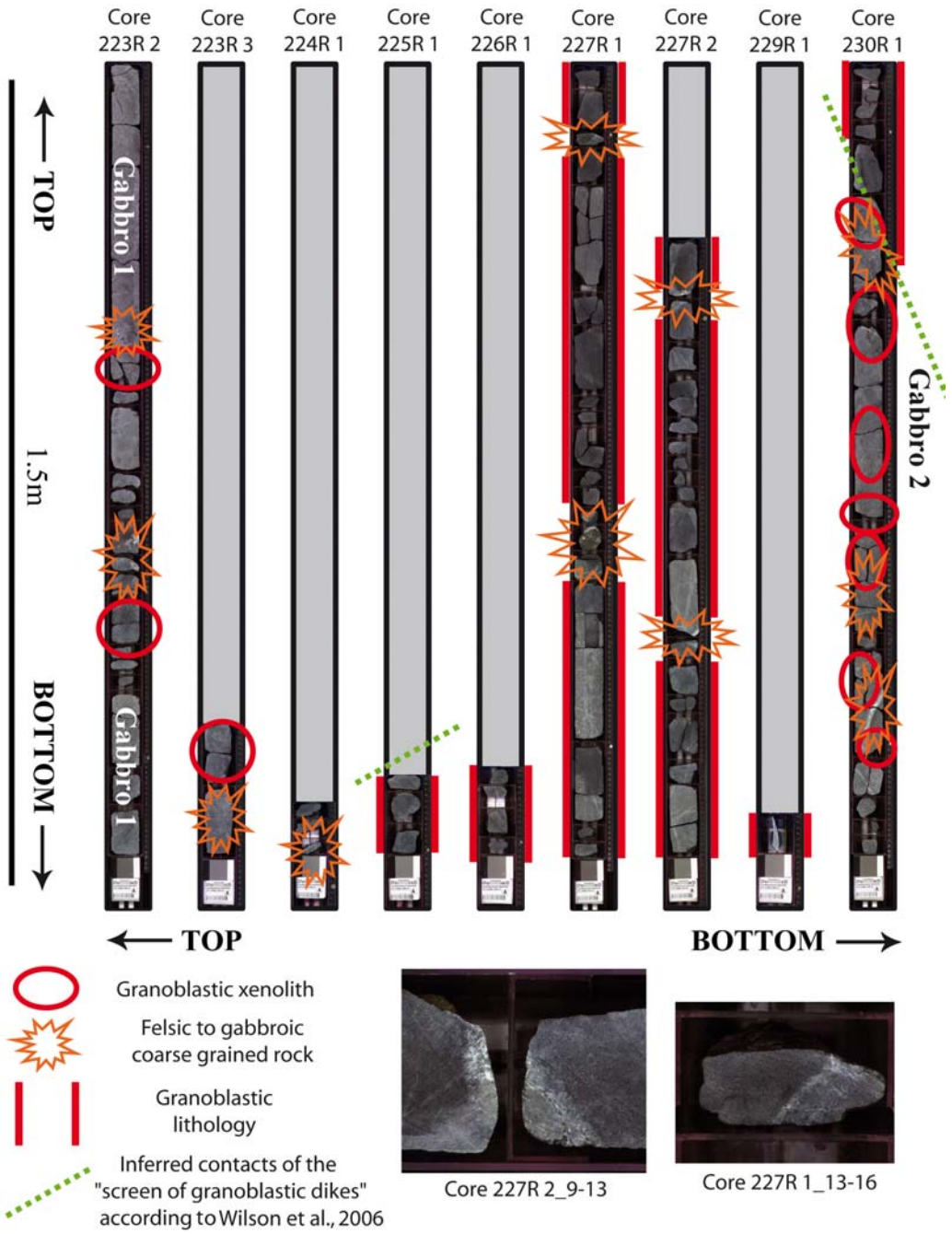

Figure 11. IODP 1256D drilled cores between 1450.8 and 1484.4 mbsf. From top to bottom, encountered lithologies are xenolith-bearing gabbro 1, granoblastic lithologies described as a "screen of granoblastic dikes" by *Wilson et al.* [2006], and xenolith-bearing gabbro 2. The two photographs show some of the felsic to mafic "melts" that crosscut the recrystallized granoblastic lithologies. Red circles highlight the xenoliths of granoblastic lithologies, and orange stars highlight the occurrence of felsic to gabbroic coarse-grained material. Intervals with recrystallized granoblastic texture are highlighted by thick red lines along the core margins. The dotted green lines represent the upper and lower limits of the "screen of granoblastic dikes" described by *Wilson et al.* [2006]. The continuous granoblastic domains are less than 1 m thick.

Small clinopyroxenes, which show petrographic features similar to those from granoblastic lithologies are characteristically low in Al, Ti, and Cr, and plot on the TiO_2 versus Al_2O_3 linear trend (Figure 13).

[25] Mineral compositions from the IODP Hole 1256D granoblastic lithologies are similar to those from the same lithologies in Oman (Table A1 and Figure 12). Plagioclase composition ranges from

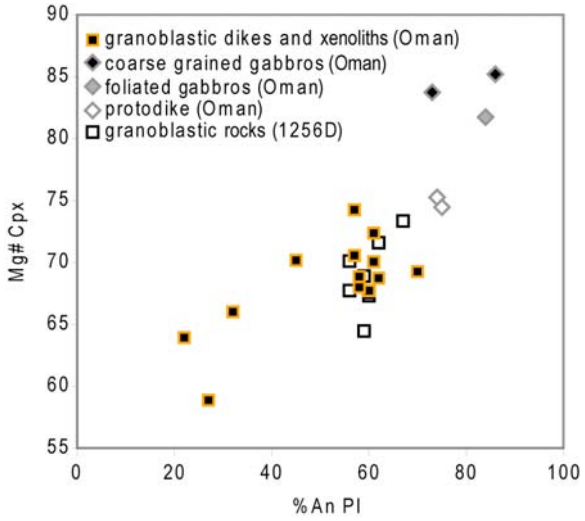

Figure 12. Mg # of clinopyroxene versus An content of plagioclases for recrystallized granoblastic dikes and xenoliths from Oman and from IODP Hole 1256D (average values for each sample). Protodike, foliated gabbro, and coarse-grained gabbro compositions are given for comparison. As low-temperature alteration has led to a late albitisation of some samples, the maximum values of the An content are used.

andesine (An_{41}) to labradorite (An_{67}). Clinopyroxenes range from augite to diopside, with Mg # between 63 and 74, low Al_2O_3 and low TiO_2 contents, high CaO content, and Cr_2O_3 always under the detection limit (Figure 13). These clinopyroxenes plot in the TiO_2 versus Al_2O_3 linear trend (Figure 13). Orthopyroxenes are enstatite, with Mg # between 58 and 66. Amphiboles are hornblende and pargasite with late actinolite.

5.2. Isotropic/Foliated Gabbro Transition in Wadi Gideah

[26] Xenolith samples contain plagioclase ranging from An_{31} to An_{57}. Clinopyroxenes are either augite or diopside, and have Mg # between 61 and 77. They are depleted in Al_2O_3 and TiO_2, and enriched in CaO; Cr_2O_3 is always under detection limits; they plot in the TiO_2 versus Al_2O_3 linear trend (Figure 13). Amphiboles are hornblende.

[27] Gabbroic samples contain olivine with Mg # of 78; plagioclases range from An_{57} to An_{86} and clinopyroxenes are mostly diopside with Mg # of 86. Clinopyroxenes have high Al_2O_3 contents and high Cr_2O_3 contents (up to ~1 wt %) and plot out of the TiO_2 versus Al_2O_3 linear trend defined by clinopyroxenes from granoblastic lithologies at the base of the sheeted dikes. Amphiboles are pargasite.

5.3. Foliated Gabbros

[28] In foliated gabbros olivine is Fo_{73}, and plagioclase is bytownite with An_{84}. Clinopyroxenes range from augite to diopside, with Mg # of 88 on average, and plot out of the TiO_2 versus Al_2O_3 linear trend defined by clinopyroxenes from the granoblastic samples. Cr_2O_3 content is 0.55 wt %, clearly above the detection limit. Amphiboles are hornblende, edenite and pargasite. In the domains of foliated gabbros that contain late orthopyroxene and pargasite rims around olivine, plagioclase is bytownite with An_{83}, clinopyroxenes are augite to diopside with Mg # of 82 in average and also plot out of the TiO_2 versus Al_2O_3 linear trend defined by granoblastic clinopyroxenes. Cr_2O_3 contents are also above the detection limit (0.17 wt %). Orthopyroxene that rims olivine is enstatite with an average Mg # of 73.

5.4. Thermometry

[29] Calculated temperatures obtained from amphibole compositions with the *Ernst and Liu* [1998] semiquantitative thermometer, from coexisting amphibole and plagioclase with the *Holland and Blundy* [1994] thermometer, and from coexisting clinopyroxenes and orthopyroxenes with the *Andersen et al.* [1993] thermometer, are summarized in Table 1. The errors on these temperature estimates are indicated in Table 1 for the two-pyroxene thermometer, are ±35–40°C for the *Holland and Blundy* [1994] thermometer, and are not estimated by *Ernst and Liu* [1998] for their semiquantitative thermometer. Temperatures obtained from amphiboles compositions reach ~1020°C with the *Ernst and Liu* [1998] thermometer, ~820°C with the *Holland and Blundy* [1994] thermometer, and are consistent with granulite facies conditions. Temperatures obtained with the *Andersen et al.* [1993] thermometer reach 1030°C in granoblastic lithologies (xenoliths and truncated dikes) and 950°C in protodikes.

6. Discussion

6.1. A Dynamic Melt Lens

[30] The occurrence of a sharp contact between sheeted dikes and underlying gabbro, with abruptly truncated sheeted dikes, and of gabbroic to oceanic plagiogranitic dikelets intruding the sheeted dike, together with the evidence that gabbroic and oceanic plagiogranitic bodies crosscut former dike margins, imply a magmatic contact that is not disturbed by

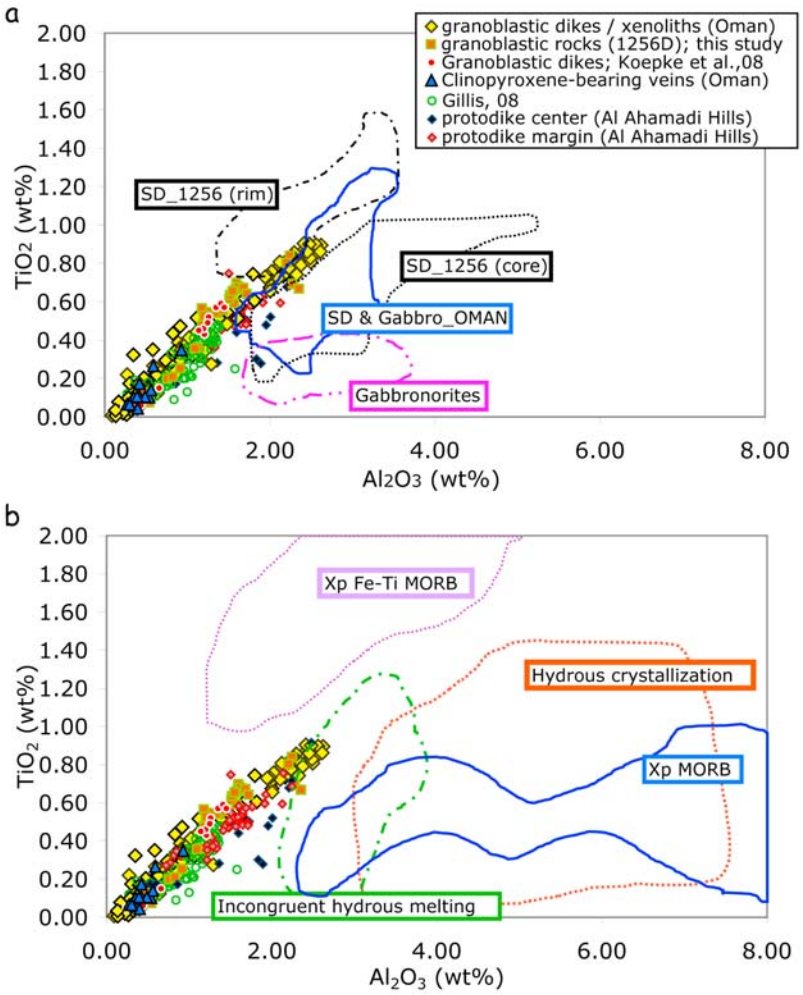

Figure 13. TiO_2 versus Al_2O_3 in clinopyroxene for recrystallized granoblastic dikes and xenoliths from Oman and from IODP Hole 1256D. Fields represent data from literature for comparison: (a) natural samples and (b) experimental samples. Natural sample data are from *Dziony et al.* [2008] for the IODP Hole 1256D sheeted dikes not affected by granoblastic imprint (SD), from *Miyashita et al.* [2003] and *Pallister and Hopson* [1981] for the Oman ophiolite sheeted dikes and gabbros, and from *Boudier et al.* [2000] and *Gerbert-Gaillard* [2002] for the Oman gabbronorites. Experimental data are from *Snyder et al.* [1993], *Toplis and Carroll* [1995], and *Toplis et al.* [1994] for Fe-Ti MORB crystallization experiments (Xp Fe-Ti MORB); from *Berndt et al.* [2005] and *Feig et al.* [2006] for hydrous crystallization experiments in primitive MORB-type system; from *Grove and Bryan* [1983] and *Kinzler and Grove* [1992] for MORB crystallization experiments (Xp MORB); and from *Koepke et al.* [2004] for clinopyroxenes formed during hydrous partial melting of gabbros. Note that the clinopyroxene in the granoblastic lithologies form a characteristic linear trend at low concentrations, which is not shown by data for typical MORB magmatic processes, neither from natural occurrences nor from experiments.

tectonics (Figure 6). This magmatic contact could be the consequence of either the upwelling of a magma body which intrudes the dikes, or hydrous partial melting of the dikes. The latter could be induced either by an injection of hydrous fluids in a still hot (>850°C) environment [*Nicolas et al.*, 2008], or by the upwelling of the magma body which reheats some previously hydrothermally altered lithologies above their hydrous solidus [e.g., *Coogan et al.*, 2003; *Wilson et al.*, 2006]. Both hydrous melting processes lead to the generation of felsic to mafic melts, depending on temperature [*Beard and Lofgren*, 1991; *Koepke et al.*, 2005b]. Observations made in Oman and in IODP Hole 1256D allow the identification of active processes in the root zone of the sheeted dike complex.

[31] The granoblastic textures at the base of the sheeted dikes could be ascribed to contact metamorphism, as proposed for IODP Hole 1256D [*Wilson et al.*, 2006; *Koepke et al.*, 2008], the Troodos ophiolite [*Gillis and Roberts*, 1999], or Wadi Him in

Table 1. Maximum An Content of Plagioclase and Temperature Estimates[a]

Lithology	Location	Sample	%An Max	T_{max} Amp (°C)	T Amp H&B (°C)	T Opx-Cpx (°C)
RZ_dike	Gideah	08OL15b-leuco	60	660	692	–
RZ_dike	Gideah	08OL15b	61	922	728	–
RZ_dike	Gideah	08OL01e	60	571	615	–
RZ_dike	Gideah	08OL04a	58	885	731	–
RZ_dike	Gideah	08OL05a	62	633	680	–
RZ_dike	Gideah	07OL51b	22	562	739	–
RZ_dike	Gideah	08OL06i	47	754	640	–
RZ_Cpx vein	Gideah	08OL15i1	70	853	711	–
RZ_dike	Al Ahmadi	08OL07b	32	650	820	–
RZ_Plagiogranite	Gideah	07OL48d	27	–		–
Granoblastic patch in isotropic gabbro	Gideah	08OL01d	58	726	784	–
Xenolith in isotropic gabbro	Gideah	08OL06f	61	998	727	–
Xenolith close to isotropic/foliated gabbro transition	Al Ahmadi	08OL29e	45	665	729	–
Xenolith close to isotropic/foliated gabbro transition	Gideah	07OL49c1	57	758	803	–
Xenolith close to isotropic/foliated gabbro transition	Gideah	07OL49b1	57	788	772	–
Coarse-grained gabbro	Gideah	07OL49d1	73	1023	811	–
Coarse-grained gabbro	Gideah	07OL49d2	86	953	683	–
Protodike border	Al Ahmadi	08OL29c	75	831	672	949 ± 40
Protodike center	Al Ahmadi	08OL29d	74	868	676	–
Foliated gabbro A	Al Ahmadi	08OL29b	87	750	701	–
Foliated gabbro B	Al Ahmadi	08OL29a	84	999	731	773 ± 18
Granoblastic dikes	1256D	312_1256D_D202R1_8-10	59	592	604	1010 ± 24
Granoblastic screen	1256D	312_1256D_D225R1_4-8	67	887	699	965 ± 77
Granoblastic screen	1256D	312_1256D_D226-R1-4-6	59	823	724	1019 ± 34
Granoblastic screen	1256D	312_1256D_D227R1_30-34	56	632	665	956 ± 77
Granoblastic xenolith in isotropic gabbro	1256D	312_1256D_D230R1_15-20	56	–		1017 ± 30
Granoblastic xenolith in isotropic gabbro	1256D	312_1256D_D230R1_73-80	60	713	769	1030 ± 35
Granoblastic xenolith in isotropic gabbro	1256D	312_1256D_D230R1_87-90	60	704	753	1028 ± 21
Lower granoblastic interval	1256D	312_1256D_D233R1_14-18	62	–		1003 ± 50

[a] Amphibole thermometer (*Ernst and Liu* [1998] (T_{max}) and *Holland and Blundy* [1994] (H&B)) and two-pyroxene thermometer [*Andersen et al.*, 1993]. Pl_c, plagioclase core; Pl_b, plagioclase rim; Amp, amphibole; ilm, ilmenite; magt, magnetite; Cpx, clinopyroxene; Chlo, chlorite; Ol, olivine; Opx, orthopyroxene; Qz, quartz.

Oman [*Gillis*, 2008]. However, in contrast to what is postulated by *Gillis* [2008], contact metamorphism is not the only process producing well-equilibrated fine-grained textures. Alternatively, *Rothery* [1983], *Nicolas and Boudier* [1991], and *Nicolas et al.* [2008] argue that microgranular textures of "protodike" margins are magmatic and represent, in a steady state system, the roots of the sheeted dikes. We propose that the late dikes described herein correspond to such protodikes. However, several features described in the dikes truncated by gabbro and in granoblastic xenoliths depart from the protodike description:

[32] 1. The core of truncated dikes is also granoblastic (Figures 7b and 9d) while the core of protodikes is described as texturally close to isotropic ophitic gabbro [*Nicolas et al.*, 2008] (Figure 9f).

[33] 2. All granoblastic xenoliths and truncated dikes described in this study contain either high oxide concentrations (up to 10% of ilmenite + magnetite), or numerous oxide inclusions in pyroxenes, or both (Figures 7, 9c, and 9d). The observed oxide concentrations depart from the published protodike descriptions [see, e.g., *Nicolas et al.*, 2008, Figure 6a], and the occurrence of numerous tiny oxides inclusions in the clinopyroxenes of granoblastic lithologies is interpreted as a consequence of the granulitic overprint of previously hydrothermally altered dike rocks. *Koepke et al.* [2008] described the evolution of the granoblastic metamorphism in the drilled core from site 1256D and show that similar clinopyroxenes with oxide inclusions, present in the granoblastic dikes from IODP Hole 1256D, recrystallized from former amphiboles. In Oman, the occurrence of veins composed of oxide-bearing clinopyroxenes at the base of the truncated granoblastic sheeted dikes (Figures 7g and 7h) also points to a metamorphic origin. Amphibole-bearing hydrothermal veins are common at the base of the sheeted dike complex, but magmatic clinopyroxenite veins have not been described. We postulate here that these peculiar veins result from the recrystallization of amphibole-bearing hydrothermal veins through dehydration reactions during a reheating episode.

[34] 3. Clinopyroxenes from the prograde veins have compositions similar to those in the granoblastic dikes and xenoliths (Table A1 and Figure 13). They are poor in Al_2O_3, rich in CaO and plot in the TiO_2 versus Al_2O_3 linear trend defined by granoblastic clinopyroxenes (Figure 13). These compositions clearly differ from published ones for magmatic natural and experimental clinopyroxenes in oceanic lithologies (Figure 13). Such compositions with uncommon low Al_2O_3 contents may indicate, as shown by *Spear and Markussen* [1997], inframagmatic temperature equilibration (<1000°C), and are consistent with granulite facies conditions. The correlation of Al_2O_3 with TiO_2 could be explained by the fact that Ti stability in clinopyroxene is linked to its Al content [*Lundstrom et al.*, 1998]. The very low Cr_2O_3 content (always under detection limits) also supports the metamorphic origin of these minerals, as magmatic oceanic pyroxenes contain higher amounts of Cr [*Koepke et al.*, 2008]. An incongruent origin linked to low degrees of hydrous partial melting of previously hydrothermally altered dikes may also be proposed as it would also result in the destabilization and dehydration of amphibole-bearing lithologies.

[35] All granoblastic xenoliths and truncated dikes have similar petrological and geochemical characteristics, which are clearly different from protodikes. Their occurrence attests to a reheating stage that we relate to the upwelling of the top of the melt lens. The presence of granoblastic xenoliths and patches in the isotropic ophitic gabbros, which are believed to represent some reheated pieces of previously hydrothermally altered sheeted dike, attests to assimilation processes, and is consistent with an upwelling stage. Upward migration of the melt lens summit can be triggered either by an upward migration of the whole melt lens, or by an inflation of its volume. Alternatively, the intrusive contact of gabbro with sheeted dikes, and associated reheating could be related to the off-axis injection of a new melt lens, as recently imaged at the East Pacific Rise by *Canales et al.* [2008].

[36] The common occurrence of leucocratic rocks (oceanic plagiogranites) at the contact between the sheeted dikes and the underlying gabbros may be related either to differentiation at the top of the melt lens or to hydrous partial melting of the sheeted dikes [*Pedersen and Malpas*, 1984; *Beard and Lofgren*, 1991]. In the present case, because reheating and magma upwelling are documented, and temperatures up to 920°C and 1000°C are calculated for the granoblastic dikes and the xenoliths, respectively, leucocratic rocks are likely generated by hydrous partial melting induced by reheating of hydrothermally altered dikes. This hypothesis is also supported by the occurrence, in the oceanic plagiogranites, of relic pyroxenes that are chemically identical to those of the reheated granoblastic dikes (Table A1). The reverse zoning observed in

plagioclases at the base of one granoblastic dike in Wadi Gideah may result from an early hydrothermal alteration stage leading to the albitisation of plagioclases (An_{22}), followed by hydrous partial melting that leads to the generation of wet dioritic melts percolating through the base of dikes and crystallizing An_{38} plagioclase rims.

[37] The late dikes (hereafter "dike 2," Figure 5) that crosscut the isotropic ophitic gabbros postdate the contact between the gabbro and the sheeted dikes, and imply the crystallization of the isotropic ophitic gabbros subsequently to a downward migration of the melt lens. Dikes 2 could either be injected from the remaining melt lens, or be injected laterally along axis, or be related to an off-axis magmatic episode. Because dikes 2 grade downward to protodikes, they must be emplaced in a still hot environment (~950°C according to the two-pyroxene thermometer), hence not far off axis. The low Al content of the clinopyroxenes present in protodikes also attests to a relatively low temperature equilibration that can correspond to subsolidus conditions. The equilibration of pyroxenes at these temperatures may result from slow cooling of the isotropic gabbro body. We interpret dikes 2 intrusion in ophitic gabbro as illustrating the downward migration of the top of the melt lens. This downward movement results in the crystallization of the isotropic ophitic gabbros, and allows injection of new dikes in this still hot environment from the underlying melt lens or laterally, along axis. The downward movement could be triggered either by downward migration of the whole melt lens or by a deflation of its volume.

[38] In Wadi Gideah, the sheeted dikes/gabbro transition is a well-defined contact that can be mapped in the field (Figure 2). We interpret the mapped contact (Figure 2c) as reflecting a ~50 m depth variation of the melt lens roof over a distance of ~150 m. However, one cannot exclude that this offset is related to a thin fault or shear zone, which is not visible due to the poor outcropping conditions between the two hills. Larger amplitude (one to several kilometers) variations of the melt lens summit depth have been documented by seismic imaging at the East Pacific Rise [*Cormier*, 1997; *Hussenoeder et al.*, 1996; *Solomon and Toomey*, 1992; *Singh et al.*, 1998]. An along-axis "fine-scale segmentation" of the melt lens reflector has been recently imaged in the 9°50N region of the East Pacific Rise [*Carbotte et al.*, 2008], and reveals comparable depth variations of tens of meters.

6.2. Stoping, Assimilation, and Coarse-Grained Gabbros

[39] In the context of magma upwelling at the root of the sheeted dikes, the occurrence of oxide-rich, granoblastic xenoliths in the isotropic ophitic gabbros is significant. Some xenoliths are located near the contact with sheeted dikes, but most of them appear to be accumulated at the base of the isotropic ophitic gabbro horizon, as seen in Al Ahmadi Hills, above the contact with foliated gabbros (Figure 8). The density of granoblastic xenoliths is ~3.02 g cm^{-3} (by considering the modal proportions from our petrological observations and crystal densities at 1000°C [*Fei*, 1995]: ~60% plagioclase, d ≈ 2.6 g cm^{-3}; ~30% clinopyroxene, d ≈ 3.3 g cm^{-3}; ~5% magnetite, d ≈ 4.9 g cm^{-3} and ~5% ilmenite, d ≈ 4.5 g cm^{-3}). Because plagioclase is the only mineral of the granoblastic assemblage that has a density lower than the estimated whole rock, and samples with plagioclase contents >60% are rare, this estimated density is a lower bound. It is significantly higher than the density of a dry basaltic melt that is thought to fill the melt lens, which is ~2.7 g cm^{-3}, (calculated with a pressure of 1 kbar and a temperature of 1100°C [e.g., *Lange and Carmichael*, 1990]). The melt density can be slightly higher if more evolved, and slightly lower if hydrous, but such melts are not expected to be dominant in the melt lens. Stoping is also controlled by the rheology of the host magma. It requires that the crystal content in the melt lens is low enough that it does not change significantly the density and viscosity of the magma. Geophysical and petrophysical studies show that underneath the melt lens is the main magma chamber, which contains on average a minimum of 80% of crystals [e.g., *Caress et al.*, 1992; *Collier and Singh*, 1997; *Singh et al.*, 1998; *Lamoureux et al.*, 1999; *Dunn et al.*, 2000; *Crawford and Webb*, 2002]. Xenoliths have therefore sunk through the mostly liquid melt lens to accumulate at its floor. These xenoliths are now observed in the lower part of the isotropic ophitic gabbros, which we must then interpret as representing the melt lens fossilized once away from the axis. As the floor of the melt lens is believed to continuously subside [e.g., *Nicolas et al.*, 2009], we speculate that the xenolith accumulation that we observe occurred close to the off-axis margin of the melt lens. Presumably, dike fragments are also stoped on axis, but they cannot be preserved as they are either fully assimilated or entrained and transposed downward within the foliated gabbros [*Boudier et al.*, 1996; *Nicolas et al.*, 2009] in which they are observed as

recrystallized microgabbronorite centimeter to decimeter thick lenses [*Boudier et al.*, 2000]. *Singh et al.* [1998] have shown that the melt lens is not continuous along the ridge axis but that it ranges from pure melt to mush. The partly crystallized zones may represent the first step toward the fossilization of the melt lens occurring when a decrease in the magmatic activity happens in a given section of the ridge.

[40] We also interpret the granoblastic patches (0.5 to 1 mm wide) in the ophitic gabbros as relics resulting from the partial assimilation of sheeted dike fragments (Figure 7c). The oxide-rich granoblastic texture of xenoliths is consistent, as described above, with a granulitic overprint, and related dehydration of previously hydrothermally altered lithologies. Enclosing gabbros contain amphiboles that record temperatures (~1020°C) higher than the hydrous solidus of gabbro, which points to the hydrated nature of the magma surrounding the xenoliths [*Koepke et al.*, 2005b; *Feig et al.*, 2006]. The concentration of coarse-grained gabbro around xenoliths (Figure 6f) is also consistent with magma hydration, as water is known to enhance crystal growth. In natural settings, high water pressure generally leads to more oxidizing conditions [e.g., *Botcharnikov et al.*, 2005]. However, the hydrated nature of magmas that produced coarse-grained gabbros is not consistent with differentiation under reducing conditions as proposed by *MacLeod and Yaouancq* [2000]. *Nicolas et al.* [2008] have proposed that coarse-grained gabbros could also be generated by the arrival of hydrothermal fluids in the root zone at high temperature (~1100–1200°C), leading to local, nearly total melting of gabbroic rocks. The coarse-grained gabbros described herein are spatially associated to granoblastic xenoliths that come from the base of the sheeted dike (~100 m above in the section), and sunk through the melt lens. Therefore, we propose an alternative process for the genesis of coarse-grained gabbro present in the studied areas that involves fluids brought by the dehydration of stoped and assimilated hydrothermally altered diabases in the melt lens. A way to test the role of recycled water in the genesis of coarse-grained gabbro would be to analyze the fluorine and chlorine contents of amphiboles [*Coogan et al.*, 2001]. Amphiboles with high chlorine contents and low fluorine contents attest to a hydrothermal origin, and the ones with low chlorine contents and high fluorine contents attest to a magmatic origin. We postulate that amphibole crystallizing from melts that are hydrated through recycling of previously hydrothermally altered dikes may have high fluorine and high chlorine contents. *Coogan* [2003] proposed that the fluids leading to the crystallization of many of the magmatic amphiboles that are present in the Oman ophiolite gabbros are brought by such recycling processes. A review of the amphibole compositions presented by *Coogan* [2003] shows that many of them are fluorine and chlorine rich (>1000 ppm), which is consistent with our hypothesis. *Gillis et al.* [2003] show that magmatic amphiboles from fast spreading ridges are chlorine enriched regarding the ones from slow spreading ridges; it also argues for important recycling of hydrothermally altered lithologies at fast spreading centers.

[41] Another consequence of stoping and assimilation of hydrothermally altered diabases is the geochemical contamination of the melt lens. Assimilation processes in the melt lens should have a significant effect on the composition of the melts, in particular for volatile elements [*Gillis et al.*, 2003]. Our results are consistent with the model [*Coogan et al.*, 2003], which states, from the chlorine content of EPR basalts [e.g., *Michael and Schilling*, 1989; *Michael and Cornell*, 1998], that ~20% of the oceanic crust may go through a cycle of crystallization, alteration, and assimilation.

6.3. Comparison With IODP Hole 1256D

[42] Many features in IODP Hole 1256D match the observations made in the Oman ophiolite. In particular, the root of the sheeted dike complex is recrystallized to granoblastic textures, oceanic plagiogranites are present close to the dike root zone, the isotropic ophitic gabbro horizon contains granoblastic xenoliths and patches, and the compositions of minerals that form the granoblastic textures are similar to Oman ones (Table A1 and Figures 10–13). IODP Hole 1256D can therefore be included in the same general model for the melt lens dynamics and for the relationships between the hydrothermal and magmatic systems.

[43] In the Al Ahmadi Hills section, large xenoliths (up to 1.5 m) displaying granoblastic textures are observed close to the isotropic ophitic gabbros/foliated gabbros transition, and are highly concentrated in some areas. These xenoliths can be partly assimilated by enclosing gabbro, and be associated to felsic melts at their border. In IODP Hole 1256D, the ~20 m thick "screen of granoblastic dikes" located ~50 m below the sheeted dike/gabbro contact [*Wilson et al.*, 2006] is poorly recovered (<30%), and several thin horizons of gabbros and oceanic plagiogranites isolate larger (<1 m) granoblastic zones (Figure 11). In the light of the obser-

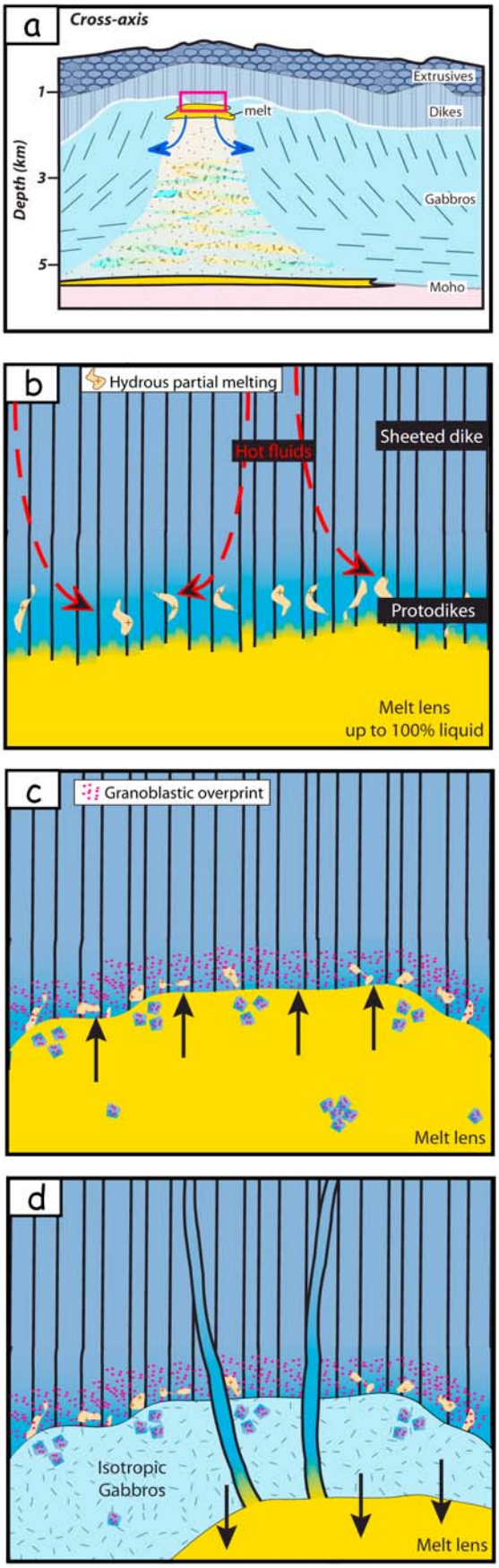

vations made in Oman, we propose that this zone may correspond to granoblastic xenoliths, surrounded by silicic to gabbroic melts, which are accumulated in the isotropic gabbro horizon about 50 m below the sheeted dike/gabbro contact. It also suggests that the bottom of Hole 1256D is close to the transition with the foliated gabbros and so to the bottom of the fossilized melt lens that would be ~100 m thick. This interpretation is in contrast with the model presented by *Koepke et al.* [2008, Figure 14c]; they interpreted the two gabbro screens as two separate intrusions into the lowermost part of the granoblastic dikes, shortly above the top of the fossilized magma chamber, which was hence not yet reached in Hole 1256D.

6.4. A general Model

[44] The model presented here elaborates on detailed mapping, sampling and descriptions made in the Wadi Gideah and Al Ahmadi Hills areas, and on subsequent petrological and geochemical study. We visited ~10 other areas in the Oman ophiolite, which are consistent with our model. As described above, observations and analyses made on samples from the sheeted dikes/gabbro transition zone in IODP Hole 1256D, are also consistent with what is observed in Oman, and with our model.

[45] The evolution of a melt lens can be tracked through the observed geological and petrological features (Figure 14). We first assume an episodic, steady state melt lens that injects dikes in the upper crust (Figure 14b). The base of these dikes is made of protodikes with microgranular margins and grade

Figure 14. General schematic model for the dynamics of the melt lens. (a) Schematic cross section at the axis of a fast spreading ridge (modified after *Sinton and Detrick* [1992]). The red rectangle indicates the location of the axial melt lens. (b) Steady state stage with injection of dikes that have at their base microgranular margins (protodikes). Hydrous partial melting is proposed to occur in the root zone of the sheeted dike complex as a result of hydrothermal fluid intrusion [*Nicolas et al.*, 2008]. (c) Upward migration of the top of the melt lens resulting in reheating and recrystallization of the base of the dikes (red dots) to granoblastic dikes and in assimilation of xenoliths in the melt lens. Hydrous partial melting of the hydrothermally altered base of the dikes can also occur. (d) Downward migration of the top of the melt lens resulting in the crystallization of the isotropic ophitic gabbros. New dikes can be injected laterally or from below; their root is typical of protodikes, with microgranular margins, and they grade upward to "classical" dikes with chilled margins (see section 6.4 for further discussion).

upward to "normal" dikes with chilled margins [*Rothery*, 1983; *Nicolas and Boudier*, 1991; *Nicolas et al.*, 2008]. In this steady state system, the injection of hydrothermal fluids in the dike root zone may trigger, locally, hydrous partial melting [*Nicolas et al.*, 2008]. This steady state system can evolve as a dynamic one with upward and downward migrations of the top of the melt lens (Figures 14c and 14d) as proposed by *Hooft et al.* [1997], *Gillis* [2002, 2008], *Gillis and Roberts* [1999], *Gillis and Coogan* [2002], *Coogan et al.* [2003], and *Koepke et al.* [2008]. These migrations can represent either vertical movements of the melt lens itself or inflation and deflation of its volume. Lateral migrations or injections may also be proposed as near-axis melt lenses have recently been observed at the East Pacific Rise [*Canales et al.*, 2008].

[46] Upward migrations or lateral intrusions can be for example triggered by magma replenishment and result in the assimilation of the hydrothermally altered dikes, with the formation of xenoliths (Figure 14c). The roof is reheated by magma upwelling, and hydrothermally altered sheeted dikes recrystallize in a granulitic granoblastic assemblage; they may locally undergo hydrous melting. Granoblastic lithologies also develop in xenoliths, which are partly to totally assimilated while sinking through the melt lens. If not totally assimilated, xenoliths sink down to the melt lens floor where they accumulate. They can then either be entrained downward in the igneous lower crust and be transposed in foliated gabbros, or be fossilized with the isotropic ophitic gabbros.

[47] Downward or lateral migrations can be triggered by a waning magmatic activity of the melt lens and/or by an eruption-related draining stage, and result in the crystallization of the isotropic gabbros at the roof and/or at the sides of the melt lens (Figure 14d). This crystallization corresponds to a partial fossilization of the melt lens which would become complete if melt supply to the melt lens was stopped.

[48] Numerous scenarios can be elaborated combining the three stages described above: steady state, upward migration of the top of the melt lens, and downward migration of the top of the melt lens. Several episodes of upward and downward migrations may alternate, and only the highest level reached by the top of the melt lens will be eventually recorded at the contact with the sheeted dike. In the case of an upward migration following a downward one, the melt lens would assimilate the recently crystallized gabbros, and the overlying recrystallized sheeted dike if the upward migration is large enough. The presence of gabbroic xenoliths in the isotropic ophitic gabbro horizon attests to this process.

6.5. Time Scale Constraints

[49] At fast spreading ridges, the time scales associated with magma migration, its residence within the main magma chamber and within the melt lens, and depth variations of the melt lens represent major parameters of the dynamics of oceanic crust formation. Unfortunately these time scales remain poorly constrained. We compile here published data dealing with these different time scales in order to replace our model on the evolution of a dynamic melt lens into a possible time frame.

[50] Seismic reflection profiles of the East Pacific Rise (EPR) at 19°S (spreading rate: ~15 cm/y [*Hooft et al.*, 1997]) suggest variations in the magma supply on a time scale of ~100,000 years. *Hooft et al.* [1997] also propose that spreading events like dike intrusions and eruptions occur on much shorter time scales (tens to hundred years). *Lagabrielle and Cormier* [1999] propose that elongated summit troughs present at the EPR (17–18°S, spreading rate: ~15 cm/y) represent elongated collapsed calderas that form every ~100,000 years when a given ridge section deflates as a result of waning magma supply. *Pollock et al.* [2009] propose, based on spatial and temporal variations of basalt MgO contents at the EPR (Pito Deep, spreading rate: ~14 cm/y), that the magmatic temperatures, hence the magma supply, remain constant over time scales of tens of thousands of years, suggesting a nearly continuous magma recharge of the system at that time scale. It is in agreement with the observations of *Sinton et al.* [2002] on the south EPR that suggest, based on the MgO content of successive units, that magmatic temperatures can remain constant over hundreds to tens of thousands of years.

[51] *Rannou et al.* [2006] use a mathematic model based on geochemical data to infer that the magmatic system of the EPR at 17–19°S has a replenishment period of ~750 years for a magma residence time of ~300 years. This residence time is in good agreement with the estimate of *Rubin et al.* [2005] who propose, based on ^{210}Pb-^{226}Ra-^{230}Th radioactive disequilibria on samples from the EPR at 9°N (spreading rate: ~11 cm/y) and 17°S, and from the Juan de Fuca Ridge (spreading rate: ~5.6 cm/y), that melt can be transferred within decades from the mantle to melt lens where it mixes and resides during ~200–400 years. *Rubin and Sinton* [2007]

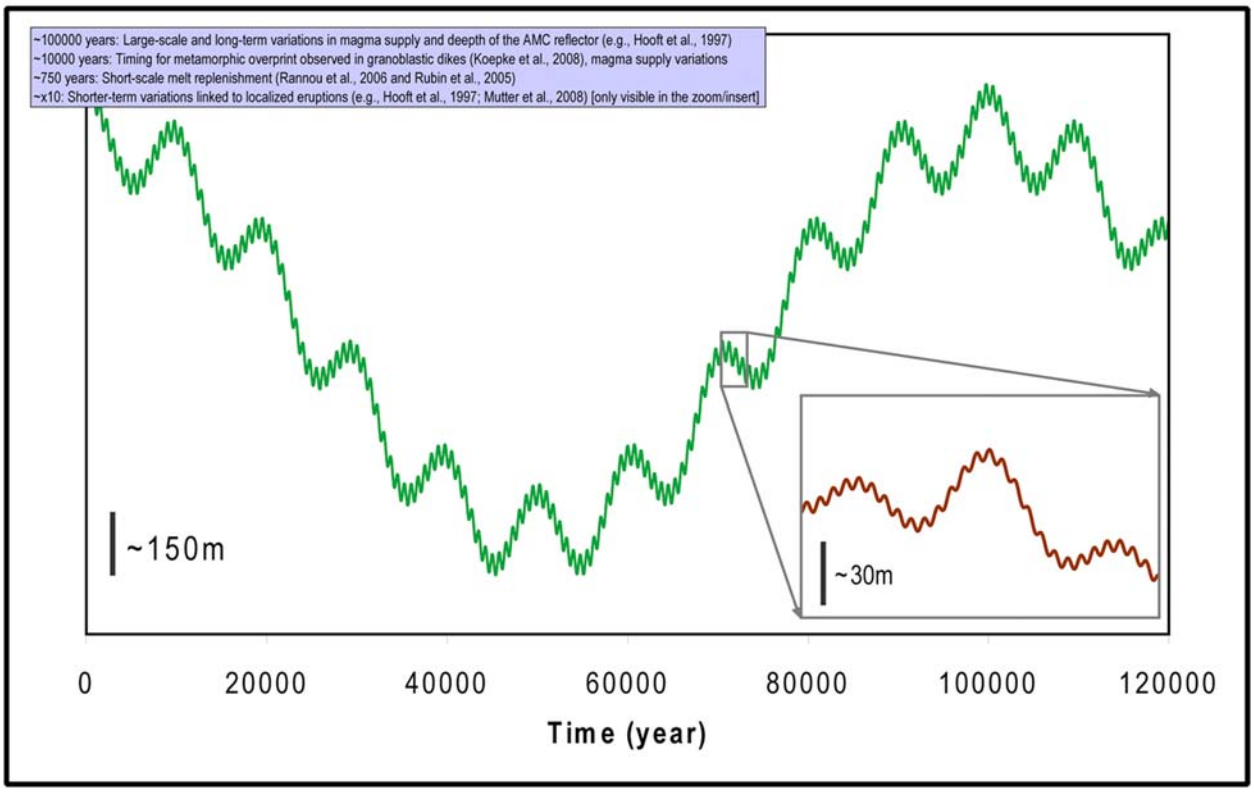

Figure 15. Compilation of estimated time scales for the dynamics of the melt lens in a depth versus time schematic graph. Four periods of depth variation are displayed (100,000, 10,000, 750, ×10 years). The insert on a portion of the curve allows the visualization of the shortest time period (×10 years). See section 6.5 for further discussion.

also propose a magma replenishment time <1000 years at fast spreading ridges. Using the chemical zonations of olivine crystals present in four samples from the EPR (9°30′N and 10°30′N), *Pan and Batiza* [2002] have proposed that magma mixing events and eruptions may be in some cases separated by times as short as a few months.

[52] Preliminary results of the recent multistreamer reflection imaging experiment in the 9°50′N region of the EPR [*Mutter et al.*, 2008] show significant variation in the depth of the melt lens reflector between 1985 and 2008 at 9°50′N, possibly as a result of the 1991 and/or 2005–2006 eruptions in that area, while there is no significant variation observed at 9°30′N and 9°40′N. *Carton et al.* [2008] report a variation in the reflectivity strength of the melt lens that they interpret as indicating a lower melt percentage between 9°45.2′N and 9°51.9′N, consistent with melt drainage during 1991 and 2005–2006 eruptions. These observations suggest that if replenishment has occurred or started since the last eruption, it is either incomplete or reduced (compared to the erupted melt volume). The timing between these events is in agreement with the time scale of ten to tens of years proposed for spreading events by *Hooft et al.* [1997]. *Sinton et al.* [2002] and *Bergmanis et al.* [2007] also propose that eruptions along intermediate to superfast spreading centers are highly episodic and have repose times of ten years to a few hundred years.

[53] *Gillis* [2008] and *Koepke et al.* [2008] have tried to estimate the duration of the thermal overprint, which we link to upward movements of the melt lens summit, by studying plagioclase zoning in granoblastic domains. *Gillis* [2008] estimates a minimum duration of 50 years for Hess Deep sample (spreading rate: ~13.5 cm/year). *Koepke et al.* [2008] propose an overprint duration of ~10,000 years for a sample from IODP Hole 1256D.

[54] In summary, multidisciplinary results provide indirect constraints on time scales for the vertical fluctuations of the melt lens ranging from a few tens of years to ~100,000 years. In Figure 15, we propose a way to take into account these apparently contrasting results and to interpret them in a single schematic model. Four different time scales, consistent with published estimates, are used to describe the evolution of the summit of the melt lens: 100,000, 10,000, 750 and tens of years (Figure 15).

These different time scales correspond to different processes and/or to different spatial scales. The long period (~100,000 years) proposed by *Hooft et al.* [1997] may represent variations in the magma supply from the mantle and correspond to variations of the depth of the melt lens in the scale of several hundreds of meters. The higher the spreading rate (hence the magma supply), the shallower the depth of the melt lens [*Purdy et al.*, 1992; *Phipps Morgan and Chen*, 1993; *Wilson et al.*, 2006]. The ~10,000 year period is identified by *Koepke et al.* [2008] and *Pollock et al.* [2009] and may correspond to temporary high positions of the melt lens related to shorter-term variations in the magma supply. The ~750 years period is the one identified by *Rannou et al.* [2006], *Rubin et al.* [2005], and *Rubin and Sinton* [2007] for the melt lens replenishment. The shortest period corresponds to local, individual eruptions [e.g., *Hooft et al.*, 1997; *Mutter et al.*, 2008]. The oscillatory evolution proposed in Figure 15 is an attempt to integrate published time scales constraints that are currently available. However, it remains schematic and probably too simplistic to illustrate natural processes. The regular oscillatory evolution is probably too simple and irregularities are likely to occur at each time scale. The very short time between magma mixing and eruptions documented by *Pan and Batiza* [2002] may be an example of such episodic irregularities. The insert in Figure 15 proposes, as an example, an irregular evolution of the 750 year period for a portion of the curve. The depth variations of the summit of the melt lens identified in the present study range from meters to several tens of meters and match the short and middle time scales ($\leq$10,000 years).

7. Conclusions

[55] New detailed mapping and petrological studies of the gabbro/sheeted dikes transition zone performed in "undisturbed" zones of the Oman ophiolite provide information about the evolution of the melt lens at fast spreading ridges. It further constrains the interactions between the magmatic system and the convective hydrothermal system at the ridge axis. The comparison of the Oman ophiolite with IODP Hole 1256D results in a global coherent model, which reconciles the apparently contrasting previous published ones (Figure 14).

[56] We assume that sheeted dikes can be injected from an episodically steady state melt lens as described by *Nicolas et al.* [2008]. However, this steady state behavior is overprinted by upward migrations of the melt lens that are documented in the Oman ophiolite and at the East Pacific Rise. These upward migrations induce reheating, dehydration, and hydrous partial melting at the roof of the melt lens, leading to the occurrence of oceanic plagiogranites and assimilation of hydrothermally altered rocks in the melt lens. These processes imply a contamination of the melt lens by silicic melts formed during hydrous partial melting and by hydrothermal fluids recycled through assimilation. Downward migrations of the top of the melt lens can also occur and result in the crystallization of the isotropic ophitic gabbros that represent a fossilized melt lens. Melt lens crystallization eventually occurs at the melt lens margins where the thermal regime is cooler.

[57] We also show that the well-equilibrated, fine-grained diabase textures observed in numerous oceanic or ophiolitic sites can have either a magmatic origin (protodikes) or a metamorphic origin (granoblastic dikes). Composition (e.g., Ti, Al, Cr in clinopyroxene), mineralogy (abundance of oxides), detailed petrographic observations (e.g., presence of clinopyroxenes with characteristic oxide inclusions), and description of associated lithologies (e.g., texture in the dike cores) are required to distinguish these two origins.

[58] At fast spreading ridges, the top of the melt lens, which corresponds to the magmatic/hydrothermal interface, should be considered as a dynamic interface. On the first order, the melt supply from the underlying main magma chamber, the occurrence of eruptions, and the vigor of the hydrothermal convecting system regulate its position. Short wavelength variations of the depth of the summit of the melt lens are observed (50 m of variation for distance of 150 m along axis).

Appendix A

[59] Mineral compositions of samples from the Oman ophiolite and from IODP Hole 1256D are presented in Table A1. FeO is the FeO total, Mg # = MgO/(MgO + FeOt) in molar proportions, and An % = CaO/(CaO + Na2O + K2O) in molar proportions; in the lithology names, RZ means root zone of the sheeted dikes. Foliated gabbro A is the "normal" foliated gabbro, and foliated gabbro B represents the foliated gabbro domains where the foliation is hardly identifiable in the field and that contain orthopyroxene and pargasite. The asterisks identifies samples analyzed in Montpellier; other samples were analyzed in Hannover. Plc means

Table A1 (Sample). Mineral Compositions of Samples From the Oman Ophiolite and From IODP Hole 1256D[a] [The full Table A1 is available in the HTML version of this article]

Sample	Zone	Lithology	Mineral	SiO_2	Al_2O_3	TiO_2	CaO	Na_2O	K_2O	MnO	MgO	FeO	Cr_2O_3	Total	Mg #	An %
08OL15b-leuco	Gideah	RZ_dike	Pumpellyite	36.07	22.70	0.30	22.36	0.06	0.01	0.08	1.51	8.89	–	91.97	–	–
08OL15b-leuco	Gideah	RZ_dike	Pumpellyite	35.94	21.81	0.19	22.75	0.07	0.00	–	1.49	9.33	0.02	91.59	–	–
08OL15b-leuco	Gideah	RZ_dike	Pumpellyite	35.93	20.15	0.10	21.96	0.06	0.01	–	1.63	10.68	0.06	90.57	–	–
08OL15b-leuco	Gideah	RZ_dike	Plc	55.22	27.73	0.08	11.06	5.51	0.07	0.06	0.03	0.51	–	100.28	–	52.60
08OL15b-leuco	Gideah	RZ_dike	Plc	54.72	28.22	0.06	11.23	5.30	0.05	0.02	0.01	0.40	–	100.02	–	53.93
08OL15b-leuco	Gideah	RZ_dike	Plc	54.40	28.12	0.06	11.38	5.26	0.07	–	0.03	0.53	0.04	99.88	–	54.46
08OL15b-leuco	Gideah	RZ_dike	Plc	54.21	28.54	0.06	11.31	5.24	0.05	–	0.00	0.43	0.06	99.89	–	54.42
08OL15b-leuco	Gideah	RZ_dike	Plc	53.84	28.81	0.06	11.42	5.04	0.12	0.03	0.06	0.54	0.04	99.94	–	55.61
08OL15b-leuco	Gideah	RZ_dike	Plc	53.18	29.33	0.04	12.26	4.57	0.07	–	0.05	0.52	0.03	100.05	–	59.71
08OL15b-leuco	Gideah	RZ_dike	Plc	53.96	28.64	0.05	11.56	5.09	0.03	–	0.03	0.44	0.00	99.80	–	55.65
08OL15b-leuco	Gideah	RZ_dike	Plc	53.85	28.37	0.06	11.40	5.49	0.06	0.05	0.02	0.51	0.00	99.81	–	53.45
08OL15b-leuco	Gideah	RZ_dike	Plc	55.56	27.79	0.06	10.08	5.98	0.09	–	0.01	0.39	0.00	99.96	–	48.21
08OL15b-leuco	Gideah	RZ_dike	Plc	53.48	28.95	0.06	11.53	5.25	0.06	0.01	0.00	0.40	0.04	99.78	–	54.84
08OL15b-leuco	Gideah	RZ_dike	Plc	52.55	29.25	0.08	12.29	4.70	0.08	0.00	0.03	0.59	0.01	99.58	–	59.10
08OL15b-leuco	Gideah	RZ_dike	Plb	64.12	22.55	0.03	3.95	9.41	0.11	0.04	0.03	0.24	0.03	100.50	–	18.82
08OL15b-leuco	Gideah	RZ_dike	Plb	63.33	22.77	0.02	4.26	9.45	0.17	0.00	0.01	0.26	0.04	100.30	–	19.92
08OL15b-leuco	Gideah	RZ_dike	Plb	63.84	22.64	0.02	4.15	9.41	0.08	–	0.01	0.38	0.06	100.58	–	19.60
08OL15b-leuco	Gideah	RZ_dike	Plb	62.82	23.62	0.02	4.95	9.11	0.09	–	0.01	0.35	0.01	100.96	–	23.09
08OL15b-leuco	Gideah	RZ_dike	Plb	62.83	23.15	0.04	4.84	8.72	0.09	0.01	0.00	0.34	0.01	100.04	–	23.49
08OL15b-leuco	Gideah	RZ_dike	Plb	63.79	23.21	0.02	4.46	9.34	0.12	0.01	0.01	0.35	0.03	101.32	–	20.86
08OL15b-leuco	Gideah	RZ_dike	Plb	64.66	22.40	0.02	3.50	10.08	0.10	–	0.00	0.32	–	101.09	–	16.10
08OL15b-leuco	Gideah	RZ_dike	Plb	61.70	24.28	0.02	5.91	8.47	0.08	–	0.01	0.36	0.02	100.86	–	27.84
08OL15b-leuco	Gideah	RZ_dike	magt	0.00	0.40	1.23	0.04	0.00	0.00	–	0.03	90.92	0.18	92.79	–	–
08OL15b-leuco	Gideah	RZ_dike	magt	0.05	0.34	1.03	0.10	–	–	0.04	–	90.53	0.25	92.33	–	–
08OL15b-leuco	Gideah	RZ_dike	magt	0.12	0.43	1.04	0.03	–	0.01	0.07	0.01	91.23	0.15	93.08	–	–
08OL15b-leuco	Gideah	RZ_dike	magt	0.07	0.40	1.02	0.06	0.02	0.01	0.07	0.02	90.22	0.09	91.99	–	–
08OL15b-leuco	Gideah	RZ_dike	ilm	0.04	0.12	40.55	0.03	0.04	0.00	1.48	0.06	51.99	0.04	94.37	–	–
08OL15b-leuco	Gideah	RZ_dike	ilm	0.10	0.08	44.13	0.03	0.00	–	1.77	0.08	48.78	0.02	94.98	–	–
08OL15b-leuco	Gideah	RZ_dike	ilm	0.02	0.04	46.43	0.05	–	0.00	1.28	0.01	49.73	0.05	97.61	–	–
08OL15b-leuco	Gideah	RZ_dike	ilm	–	0.05	46.75	0.03	0.00	0.01	1.33	0.10	49.56	0.00	97.83	–	–
08OL15b-leuco	Gideah	RZ_dike	ilm	0.02	0.06	47.13	–	0.03	–	1.57	0.08	48.39	0.00	97.28	–	–
08OL15b-leuco	Gideah	RZ_dike	Apatite	0.18	0.02	–	54.52	0.03	0.00	0.06	–	0.08	0.03	54.92	–	–
08OL15b-leuco	Gideah	RZ_dike	Amp	51.79	2.70	0.30	9.50	0.38	0.04	0.46	14.72	17.21	–	97.11	62.99	–
08OL15b-leuco	Gideah	RZ_dike	Amp	51.02	3.94	0.35	11.94	0.59	0.04	0.28	13.85	16.16	–	98.17	65.04	–
08OL15b-leuco	Gideah	RZ_dike	Amp	52.55	3.72	0.28	10.67	0.29	0.06	0.40	13.89	15.39	0.05	97.29	62.12	–
08OL15b-leuco	Gideah	RZ_dike	Amp	50.86	3.91	0.32	11.42	0.66	0.07	0.31	13.47	17.10	0.07	98.18	62.87	–
08OL15b-leuco	Gideah	RZ_dike	Amp	49.98	4.82	0.32	11.00	0.76	0.07	0.32	12.47	17.66	–	97.40	59.89	–
08OL15b-leuco	Gideah	RZ_dike	Amp	51.44	2.65	0.28	7.95	0.43	0.06	0.61	14.03	20.17	0.04	97.66	57.60	–
08OL15b-leuco	Gideah	RZ_dike	Amp	51.39	3.36	0.43	11.08	0.56	0.10	0.45	13.53	16.85	0.04	97.79	62.05	–

[a] FeO is the FeO total, Mg # = MgO/(MgO + FeOt) in molar proportions, An % = CaO/(CaO + Na_2O + K_2O) in molar proportions. In the lithology names, RZ means root zone of the sheeted dikes. Foliated gabbro A is the "normal" foliated gabbro, and foliated gabbro B represents the foliated gabbro domains where the foliation is hardly identifiable in the field and that contain orthopyroxene and pargasite. The asterisks identify samples analyzed in Montpellier; other samples were analyzed in Hannover. Pl_c, plagioclase core; Pl_b, plagioclase rim; Amp, amphibole; ilm, ilmenite; magt, magnetite; Cpx, clinopyroxene; Chlo, chlorite; Ol, olivine; Opx, orthopyroxene; Qz, quartz.

plagioclase core, Plb means plagioclase rim, Amp means amphibole, ilm means ilmenite, magt means magnetite, Cpx means clinopyroxene, Chlo means chlorite, Ol means olivine, Opx means orthopyroxene, and Qz means quartz.

Acknowledgments

[60] We wish to thank Adolphe Nicolas and Françoise Boudier for their dedicated assistance in the field during the first field season spent by Lydéric France in Oman and for many discussions in the lab. Christian Nicollet is also thanked for his help in the field and for discussions. Many thanks to Christine Laverne for allowing us to examine her thin sections from IODP Hole 1256D and for her unique expertise in low-temperature alteration mineralogy. We express our warm thanks to the various people involved at different technical stages of this work: Christophe Nevado, Dorianne Delmas, and Otto Diedrich for their beautiful thin sections and Claude Merlet and Wanja Dziony for their assistance during the microprobe analyses. The manuscript benefited from thorough reviews by Laurence Coogan, John MacLennan. This research used samples and data provided by the Integrated Ocean Drilling Program (IODP). Funding for this research was provided by CNRS-INSU program 3F and by the Université Franco-Allemande/Deutsch-Französische Hochchule. We thank Salim Al Busaidi, Director General of Minerals, Ministry of Commerce and Industry of the Sultanate of Oman, for allowing us to conduct this research work in the Oman ophiolite.

References

Adachi, Y., and S. Miyashita (2003), Geology and petrology of the plutonic complexes in the Wadi Fizh area: Multiple magmatic events and segment structure in the northern Oman ophiolite, *Geochem. Geophys. Geosyst.*, *4*(9), 8619, doi:10.1029/2001GC000272.

Alt, J. C., D. A. H. Teagle, S. Umino, S. Miyashita, N. R. Banerjee, D. S. Wilson, the IODP Expeditions 309 and 312 Scientists, and the ODP Leg 206 Scientific Party (2007), IODP Expeditions 309 and 312 drill an intact upper oceanic basement into gabbros, *Sci. Drill.*, *4*, 4–10, doi:10.2204/iodp.sd.4.01.2007.

Andersen, D. J., D. H. Lindsley, and P. M. Davidson (1993), QUILF: A Pascal program to assess equilibria among Fe-Mg-Mn-Ti oxides, pyroxenes, olivine, and quartz, *Comput. Geosci.*, *19*, 1333–1350, doi:10.1016/0098-3004(93)90033-2.

Beard, J. S., and G. E. Lofgren (1991), Dehydration melting and water-saturated melting of basaltic and andesitic greenstones and amphibolites at 1, 3, and 6.9 kb, *J. Petrol.*, *32*, 365–401, doi:10.1093/petrology/32.2.365.

Bergmanis, E. C., J. Sinton, and K. H. Rubin (2007), Recent eruptive history and magma reservoir dynamics on the southern East Pacific Rise at 17°30′S, *Geochem. Geophys. Geosyst.*, *8*, Q12O06, doi:10.1029/2007GC001742.

Berndt, J., J. Koepke, and F. Holtz (2005), An experimental investigation of the influence of water and oxygen fugacity on differentiation of MORB at 200 MPa, *J. Petrol.*, *46*, 135–167, doi:10.1093/petrology/egh066.

Botcharnikov, R. E., J. Koepke, F. Holtz, C. McCammon, and M. Wilke (2005), The effect of water activity on the oxidation and structural state of Fe in a ferro-basaltic melt, *Geochim. Cosmochim. Acta*, *69*, 5071–5085, doi:10.1016/j.gca.2005.04.023.

Boudier, F., A. Nicolas, and B. Ildefonse (1996), Magma chambers in the Oman ophiolite: Fed from the top and the bottom, *Earth Planet. Sci. Lett.*, *144*, 239–250, doi:10.1016/0012-821X(96)00167-7.

Boudier, F., M. Godard, and C. Armbruster (2000), Significance of gabbronorite occurrence in the crustal section of the Semail ophiolite, *Mar. Geophys. Res.*, *21*, 307–326, doi:10.1023/A:1026726232402.

Canales, J. P., S. M. Carbotte, J. C. Mutter, M. R. Nedimovic, H. Carton, M. Xu, K. Newman, O. Aghaei, M. Marjanovic, and L. C. Stowe (2008), Discovery of off-axis melt lenses at the RIDGE-2000 East Pacific Rise integrated studies site, *Eos Trans. AGU*, *89*(53), Fall Meet. Suppl., Abstract B21A-0319.

Carbotte, S. M., J. C. Mutter, J. P. Canales, M. R. Nedimovic, H. Carton, M. Xu, K. Newman, M. Marjanovic, O. Aghaei, and L. Stowe (2008), New observations of the magmatic segmentation of the East Pacific Rise from Siquieros to Clipperton from a multi-streamer seismic reflection imaging study, *Eos Trans. AGU*, *89*(53), Fall Meet. Suppl., Abstract B21A-0320.

Caress, D. W., M. S. Burnett, and J. A. Orcutt (1992), Tomographic image of the axial low-velocity zone at 12°50′N on the East Pacific Rise, *J. Geophys. Res.*, *97*(B6), 9243–9263, doi:10.1029/92JB00287.

Carton, H., S. M. Carbotte, J. C. Mutter, J. P. Canales, M. R. Nedimovic, K. Newman, M. Marjanovic, M. Xu, O. Aghaei, and L. Stowe (2008), Characteristics of the crustal magma body in the 2005–06 eruption area at 9°50′N on the East Pacific Rise from a 3D multi-channel seismic investigation, *Eos Trans. AGU*, *89*(53), Fall Meet. Suppl., Abstract B23F-03.

Collier, J. S., and S. C. Singh (1997), Detailed structure of the top of the melt body beneath the East Pacific Rise at 9°40′N from waveform inversion of seismic reflection data, *J. Geophys. Res.*, *102*(B9), 20,287–20,304, doi:10.1029/97JB01514.

Coogan, L. A. (2003), Contaminating the lower crust in the Oman ophiolite, *Geology*, *31*(12), 1065–1068, doi:10.1130/G20129.1.

Coogan, L. A., R. N. Wilson, K. M. Gillis, and C. J. MacLeod (2001), Near-solidus evolution of oceanic gabbros: Insights from amphibole geochemistry, *Geochim. Cosmochim. Acta*, *65*(23), 4339–4357, doi:10.1016/S0016-7037(01)00714-1.

Coogan, L. A., G. Thompson, and C. J. MacLeod (2002), A textural and geochemical investigation of high level gabbros from the Oman ophiolite: Implications for the role of the axial magma chamber at fast-spreading ridges, *Lithos*, *63*, 67–82, doi:10.1016/S0024-4937(02)00114-7.

Coogan, L. A., N. C. Mitchell, and M. J. O'Hara (2003), Roof assimilation at fast spreading ridges: An investigation combining geophysical, geochemical, and field evidence, *J. Geophys. Res.*, *108*(B1), 2002, doi:10.1029/2001JB001171.

Cormier, M. H. (1997), The ultrafast East Pacific Rise: Instability of the plate boundary and implications for accretionary processes, in *Mid-Ocean Ridges. Dynamics of Processes Associated With Creation of New Ocean Crust*, edited by J. R. Cann, H. Elderfield, and A. Laughton, *Philos. Trans. R. Soc. London, Ser. A*, *355*(1723), 341–367, doi:10.1098/rsta.1997.0012.

Crawford, W. C., and S. C. Webb (2002), Variations in the distribution of magma in the lower crust and at the Moho beneath the East Pacific Rise at 9°–10°N, *Earth Planet. Sci. Lett.*, *203*(1), 117–130, doi:10.1016/S0012-821X(02)00831-2.

Detrick, R. S., P. Buhl, E. Vera, J. Mutter, J. Orcutt, J. Madsen, and T. Brocher (1987), Multi-channel seismic imaging of a crustal magma chamber along the East Pacific Rise, *Nature*, *326*, 35–41, doi:10.1038/326035a0.

Dunn, R., D. Toomey, and S. Solomon (2000), Three-dimensional seismic structure and physical properties of the crust and shallow mantle beneath the East Pacific Rise at 9°30′N, *J. Geophys. Res.*, *105*(B10), 23,537–23,555, doi:10.1029/2000JB900210.

Dziony, W., J. Koepke, and F. Holtz (2008), Data report: Petrography and phase analyses in lavas and dikes from the hole 1256D (ODP Leg 206 and IODP Expedition 309, East Pacific Rise) [online], *Proc. Integrated Ocean Drill. Program*, *309/312*, 22 pp., doi:10.2204/iodp.proc.309312.201.2008. (Available at http://publications.iodp.org/proceedings/309_312/201/201_.htm)

Ernst, W. G., and J. Liu (1998), Experimental phase-equilibrium study of Al- and Ti-contents of calcic amphibole in MORB—A semiquantitative thermobarometer, *Am. Mineral.*, *83*, 952–969.

Fei, Y. (1995), Thermal expansion, in *Mineral Physics and Crystallography: A Handbook of Physical Constants*, *AGU Ref. Shelf*, vol. 2, edited by T. J. Ahrens, pp. 29–44, AGU, Washington, D. C.

Feig, S. T., J. Koepke, and J. E. Snow (2006), Effect of water on tholeiitic basalt phase equilibria: An experimental study under oxidizing conditions, *Contrib. Mineral. Petrol.*, *152*(5), 611–638, doi:10.1007/s00410-006-0123-2.

Garrido, C. J., P. B. Kelemen, and G. Hirth (2001), Variation of cooling rate with depth in lower crust formed at an oceanic spreading ridge: Plagioclase crystal size distributions in gabbros from the Oman ophiolite, *Geochem. Geophys. Geosyst.*, *2*(10), 1041, doi:10.1029/2000GC000136.

Gerbert-Gaillard, L. (2002), Caractérisation géochimique des péridotites de l'ophiolite d'Oman: Processus magmatiques aux limites lithosphère-asthénosphère, Ph.D. memoir, 241 pp., Géosci. Montpellier, Univ. Montpellier 2, Montpellier, France.

Gillis, K. M. (2002), The root zone of an ancient hydrothermal system exposed in the Troodos ophiolite, Cyprus, *J. Geol.*, *110*, 57–74, doi:10.1086/324205.

Gillis, K. M. (2008), The roof of an axial magma chamber: A hornfelsic heat exchanger, *Geology*, *36*(4), 299–302, doi:10.1130/G24590A.1.

Gillis, K. M., and L. A. Coogan (2002), Anatectic migmatites from the roof of an ocean ridge magma chamber, *J. Petrol.*, *43*(11), 2075–2095, doi:10.1093/petrology/43.11.2075.

Gillis, K. M., and M. D. Roberts (1999), Cracking at the magma-hydrothermal transition: Evidence from the Troodos ophiolite, Cyprus, *Earth Planet. Sci. Lett.*, *169*, 227–244, doi:10.1016/S0012-821X(99)00087-4.

Gillis, K. M., L. A. Coogan, and M. Chaussidon (2003), Volatile element (B, Cl, F) behaviour in the roof of an axial magma chamber from the East Pacific Rise, *Earth Planet. Sci. Lett.*, *213*, 447–462, doi:10.1016/S0012-821X(03)00346-7.

Grove, T. L., and W. B. Bryan (1983), Fractionation of pyroxene-phyric MORB at low pressure: An experimental study, *Contrib. Mineral. Petrol.*, *84*, 293–309, doi:10.1007/BF01160283.

Harding, A. J., J. A. Orcutt, M. E. Kappus, E. E. Vera, J. C. Mutter, P. Buhl, R. S. Detrick, and T. M. Brocher (1989), Structure of young oceanic crust at 13°N on the East Pacific Rise from expanding spread profiles, *J. Geophys. Res.*, *94*(B9), 12,163–12,196, doi:10.1029/JB094iB09p12163.

Henstock, T. J., A. W. Woods, and R. S. White (1993), The accretion of oceanic crust by episodic sill intrusion, *J. Geophys. Res.*, *98*, 4143–4161, doi:10.1029/92JB02661.

Holland, T., and J. Blundy (1994), Non-ideal interactions in calcic amphiboles and their bearing on amphibole-plagioclase thermometry, *Contrib. Mineral. Petrol.*, *116*, 433–447, doi:10.1007/BF00310910.

Hooft, E. E. E., R. S. Detrick, and G. M. Kent (1997), Seismic structure and indicators of magma budget along the southern East Pacific Rise, *J. Geophys. Res.*, *102*(B12), 27,319–27,340, doi:10.1029/97JB02349.

Hopson, C. A., R. G. Coleman, R. T. Gregory, J. S. Pallister, and E. H. Bailey (1981), Geologic section through the Samail ophiolite and associated rocks along a Muscat-Ibra transect, southeastern Oman mountains, *J. Geophys. Res.*, *86*, 2527–2544, doi:10.1029/JB086iB04p02527.

Hussenoeder, S. A., J. A. Collins, G. M. Kent, R. S. Detrick, A. J. Harding, J. A. Orcutt, J. C. Mutter, and P. Buhl (1996), Seismic analysis of the axial magma chamber reflector along the southern East Pacific Rise from conventional reflection profiling, *J. Geophys. Res.*, *101*(B10), 22,087–22,105, doi:10.1029/96JB01907.

Juteau, T., M. Beurrier, R. Dahl, and P. Nehlig (1988), Segmentation at a fossil spreading center: The plutonic sequence of the Wadi Haymiliyah area (Haylayn block, Sumail nappe, Oman), *Tectonophysics*, *151*, 167–197, doi:10.1016/0040-1951(88)90245-4.

Kelemen, P. B., K. Koga, and N. Shimizu (1997), Geochemistry of gabbro sills in the crust/mantle transition zone of the Oman ophiolite: Implications for the origin of the lower oceanic crust, *Earth Planet. Sci. Lett.*, *146*, 475–488, doi:10.1016/S0012-821X(96)00235-X.

Kent, G. M., A. J. Harding, and J. A. Orcutt (1990), Evidence for a smaller magma chamber beneath the East Pacific Rise at 9°30′N, *Nature*, *344*(6267), 650–653, doi:10.1038/344650a0.

Kinzler, R. J., and T. L. Grove (1992), Primary magmas of mid-ocean ridge basalts: 1. Experiments and methods, *J. Geophys. Res.*, *97*(B5), 6885–6906, doi:10.1029/91JB02840.

Klein, E. M. (2003), Geochemistry of the igneous ocean crust, in *Treatise on Geochemistry*, vol. 3, *The Crust*, edited by R. Rudnick, pp. 433–463, doi:10.1016/B0-08-043751-6/03030-9, Elsevier, Amsterdam.

Koepke, J., S. T. Feig, J. Snow, and M. Freise (2004), Petrogenesis of oceanic plagiogranites by partial melting of gabbros: An experimental study, *Contrib. Mineral. Petrol.*, *146*, 414–432, doi:10.1007/s00410-003-0511-9.

Koepke, J., S. Feig, and J. Snow (2005a), Late stage magmatic evolution of oceanic gabbros as a result of hydrous partial melting: Evidence from the Ocean Drilling Program (ODP) Leg 153 drilling at the Mid-Atlantic Ridge, *Geochem. Geophys. Geosyst.*, *6*, Q02001, doi:10.1029/2004GC000805.

Koepke, J., S. T. Feig, and J. Snow (2005b), Hydrous partial melting within the lower oceanic crust, *Terra Nova*, *17*, 286–291, doi:10.1111/j.1365-3121.2005.00613.x.

Koepke, J., D. M. Christie, W. Dziony, F. Holtz, D. Lattard, J. Maclennan, S. Park, B. Scheibner, T. Yamasaki, and S. Yamazaki (2008), Petrography of the Dike/Gabbro Transition at IODP Site 1256 (Equatorial Pacific): The evolution of the Granoblastic Dikes, *Geochem. Geophys. Geosyst.*, *9*, Q07O09, doi:10.1029/2008GC001939.

Lagabrielle, Y., and M. H. Cormier (1999), Formation of large summit troughs along the East Pacific Rise as collapse calderas: An evolutionary model, *J. Geophys. Res.*, *104*(B6), 12,971–12,988, doi:10.1029/1999JB900015.

Lamoureux, G., B. Ildefonse, and D. Mainprice (1999), Modelling the seismic properties of fast-spreading ridge crustal low-velocity zones: Insights from Oman gabbro textures, *Tectonophysics*, *312*(2–4), 283–301, doi:10.1016/S0040-1951(99)00183-3.

Lange, R. L., and I. S. E. Carmichael (1990), Thermodynamic properties of silicate liquids with emphasis on density, thermal expansion and compressibility, *Rev. Mineral. Geochem.*, *24*(1), 25–64.

Lundstrom, C. C., H. F. Shaw, F. J. Ryerson, Q. Williams, and J. Gill (1998), Crystal chemical control of clinopyroxene-melt partitionning in the Di-Ab-An system: Implications for elemental fractionations in the depleted mantle, *Geochim. Cosmochim. Acta*, *62*(16), 2849–2862, doi:10.1016/S0016-7037(98)00197-5.

MacLeod, C. J., and D. A. Rothery (1992), Ridge axial segmentation in the Oman ophiolite: Evidence from along-strike variations in the sheeted dyke complex, in *Ophiolites and Their Modern Analogues*, edited by L. M. Parson, B. J. Murton, and P. Browning, *Geol. Soc. Spec. Publ.*, *60*, 39–63, doi:10.1144/GSL.SP.1992.060.01.03.

MacLeod, C. J., and G. Yaouancq (2000), A fossil melt lens in the Oman ophiolite: Implications for magma chamber processes at fast spreading ridges, *Earth Planet. Sci. Lett.*, *176*, 357–373, doi:10.1016/S0012-821X(00)00020-0.

Merlet, C. (1994), An accurate computer correction program for quantitative electron probe microanalysis, *Mikrochim. Acta*, *114–115*, 363–376, doi:10.1007/BF01244563.

Michael, P. J., and W. C. Cornell (1998), Influence of spreading rate and magma supply on crystallization and assimilation beneath mid-ocean ridges: Evidence from chlorine and major element chemistry of mid-ocean ridge basalts, *J. Geophys. Res.*, *103*, 18,325–18,356, doi:10.1029/98JB00791.

Michael, P. J., and J. G. Schilling (1989), Chlorine in mid-ocean ridge magmas: Evidence for assimilation of seawater-influenced components, *Geochim. Cosmochim. Acta*, *53*, 3131–3143, doi:10.1016/0016-7037(89)90094-X.

Miyashita, S., Y. Adachi, and S. Umino (2003), Along-axis magmatic system in the northern Oman ophiolite: Implications of compositional variation of the sheeted dike complex, *Geochem. Geophys. Geosyst.*, *4*(9), 8617, doi:10.1029/2001GC000235.

Morton, J. L., and N. H. Sleep (1985), Seismic reflections from a Lau basin magma chamber, in *Geology and Offshore Resources of Pacific Island Arcs—Tonga Region*, edited by D. W. Scholl and T. L. Vallier, pp. 441–453, Circum-Pac. Counc. for Energy and Miner. Resour., Houston, Tex.

Mutter, J. C., H. Carton, S. M. Carbotte, J. P. Canales, M. R. Nedimovic, K. R. Newman, M. Marjanovic, M. Xu, O. Aghaei, and L. C. Stowe (2008), Searching for changes in AMC characteristics on the EPR using comparisons of reflection images obtained in 1985 and 2008, *Eos Trans. AGU*, *89*(53), Fall Meet. Suppl., Abstract B21A-0319.

Natland, J. H., and H. J. B. Dick (1996), Melt migration through high-level gabbroic cumulates of the East Pacific Rise at Hess Deep: The origin of magma lenses and the deep crustal structure of fast-spreading ridges, *Proc. Ocean Drill Program Sci. Results*, *147*, 21–58, doi:10.2973/odp.proc.sr.147.002.1996.

Nicolas, A. (1989), *Structures of Ophiolites and Dynamics of Oceanic Lithosphere*, 367 pp., Kluwer, Boston, Mass.

Nicolas, A., and F. Boudier (1991), Rooting of the sheeted dike complex in the Oman ophiolite, in *Ophiolite Genesis and Evolution of the Oceanic Lithosphere*, edited by T. Peters, A. Nicolas, and R. G. Coleman, pp. 39–54, Kluwer Acad., Dordrecht, Netherlands.

Nicolas, A., and F. Boudier (1995), Mapping oceanic ridge segments in Oman ophiolites, *J. Geophys. Res.*, *100*(B4), 6179–6197, doi:10.1029/94JB01188.

Nicolas, A., G. Ceuleneer, F. Boudier, and M. Misseri (1988a), Structural mapping in the Oman ophiolites: Mantle diapirism along an oceanic ridge, *Tectonophysics*, *151*, 27–56, doi:10.1016/0040-1951(88)90239-9.

Nicolas, A., I. Reuber, and K. Benn (1988b), A new magma chamber model based on structural studies in the Oman ophiolite, *Tectonophysics*, *151*, 87–105, doi:10.1016/0040-1951(88)90242-9.

Nicolas, A., F. Boudier, B. Ildefonse, and E. Ball (2000), Accretion of Oman and United Arab Emirates ophiolite: Discussion of a new structural map, *Mar. Geophys. Res.*, *21*, 147–179, doi:10.1023/A:1026769727917.

Nicolas, A., D. Mainprice, and F. Boudier (2003), High-temperature seawater circulation throughout crust of oceanic ridges: A model derived from the Oman ophiolites, *J. Geophys. Res.*, *108*(B8), 2371, doi:10.1029/2002JB002094.

Nicolas, A., F. Boudier, J. Koepke, L. France, B. Ildefonse, and C. Mevel (2008), Root zone of the sheeted dike complex in the Oman ophiolite, *Geochem. Geophys. Geosyst.*, *9*, Q05001, doi:10.1029/2007GC001918.

Nicolas, A., F. Boudier, and L. France (2009), Subsidence in magma chamber and the development of magmatic foliation in Oman ophiolite gabbros, *Earth Planet. Sci. Lett.*, *284*, 76–87, doi:10.1016/j.epsl.2009.04.012.

Pallister, J. S., and C. A. Hopson (1981), Samail Ophiolite Plutonic Suite: Field relations, phase variation, cryptic variation and layering, and a model of a spreading ridge magma chamber, *J. Geophys. Res.*, *86*(B4), 2593–2644, doi:10.1029/JB086iB04p02593.

Pan, Y., and R. Batiza (2002), Mid-ocean ridge magma chamber processes: Constraints from olivine zonation in lavas from the East Pacific Rise at 9°30′N and 10°30′N, *J. Geophys. Res.*, *107*(B1), 2022, doi:10.1029/2001JB000435.

Pedersen, R. B., and J. Malpas (1984), The origin of oceanic plagiogranites from the Karmoy ophiolite, western Norway, *Contrib. Mineral. Petrol.*, *88*, 36–52, doi:10.1007/BF00371410.

Phipps Morgan, J., and Y. J. Chen (1993), The genesis of oceanic crust: Magma injection, hydrothermal circulation, and crustal flow, *J. Geophys. Res.*, *98*(B4), 6283–6297, doi:10.1029/92JB02650.

Pollock, M. E., E. M. Klein, J. A. Karson, and D. S. Coleman (2009), Compositions of dikes and lavas from the Pito Deep Rift: Implications for crustal accretion at superfast spreading centers, *J. Geophys. Res.*, *114*, B03207, doi:10.1029/2007JB005436.

Pouchou, J. L., and F. Pichoir (1991), Quantitative analysis of homogeneous or stratified microvolumes applying the model "PAP," in *Electron Probe Quantification*, edited by K. F. J. Heinrich and D. E. Newbury, pp. 31–75, Plenum, New York.

Purdy, G. M., L. S. L. Kong, G. L. Christeson, and S. C. Salomon (1992), Relationship between spreading rate and the seismic structure of mid-ocean ridges, *Nature*, *355*, 815–817, doi:10.1038/355815a0.

Quick, J. E., and R. P. Denlinger (1993), Ductile deformation and the origin of layered gabbro in ophiolites, *J. Geophys. Res.*, *98*, 14,015–14,027, doi:10.1029/93JB00698.

Rannou, E., M. Caroff, and C. Cordier (2006), A geochemical approach to model periodically replenished magma chambers: Does oscillatory supply account for the magmatic evolution of EPR 17–19°S?, *Geochim. Cosmochim. Acta*, *70*, 4783–4796, doi:10.1016/j.gca.2006.07.007.

Rothery, D. A. (1983), The base of a sheeted dyke complex, Oman ophiolite: Implications for magma chambers at oceanic spreading axes, *J. Geol. Soc.*, *140*, 287–296, doi:10.1144/gsjgs.140.2.0287.

Rubin, K. H., and J. M. Sinton (2007), Inferences on mid-ocean ridge thermal and magmatic structure from MORB compositions, *Earth Planet. Sci. Lett.*, *260*, 257–276, doi:10.1016/j.epsl.2007.05.035.

Rubin, K. H., I. Van des Zander, M. C. Smith, and E. C. Bergmanis (2005), Minimum speed limit for ocean ridge magmatism from ^{210}Pb–^{226}Ra–^{230}Th disequilibria, *Nature*, *437*, 534–538, doi:10.1038/nature03993.

Sauerzapf, U., D. Lattard, M. Burchard, and R. Engelmann (2008), The titanomagnetite-ilmenite equilibrium: New experimental data and thermo-oxybarometric application to the crystallization of basic to intermediate rocks, *J. Petrol.*, *49*, 1161–1185, doi:10.1093/petrology/egn021.

Singh, S. C., G. M. Kent, J. S. Collier, A. J. Harding, and J. A. Orcutt (1998), Melt to mush variations in crustal magma properties along the ridge crest at the southern East Pacific Rise, *Nature*, *394*(6696), 874–878, doi:10.1038/29740.

Sinton, J. M., and R. S. Detrick (1992), Mid-ocean ridge magma chambers, *J. Geophys. Res.*, *97*, 197–216, doi:10.1029/91JB02508.

Sinton, J., E. Bergmanis, K. Rubin, R. Batiza, T. K. P. Gregg, K. Grönvold, K. C. Macdonald, and S. M. White (2002), Volcanic eruptions on midocean ridges: New evidence from the superfast spreading East Pacific Rise, 17°–19°S, *J. Geophys. Res.*, *107*(B6), 2115, doi:10.1029/2000JB000090.

Sleep, N. H. (1975), Formation of oceanic crust: Some thermal constraints, *J. Geophys. Res.*, *80*(B29), 4037–4042, doi:10.1029/JB080i029p04037.

Snyder, D., I. S. E. Carmichael, and R. A. Wiebe (1993), Experimental study of liquid evolution in an Fe-rich, layered mafic intrusion: Constraints of Fe-Ti oxide precipitation on the T-fO_2 and T-ρ paths of tholeiitic magmas, *Contrib. Mineral. Petrol.*, *113*, 73–86, doi:10.1007/BF00320832.

Solomon, S. C., and D. R. Toomey (1992), The structure of mid-ocean ridges, *Annu. Rev. Earth Planet. Sci.*, *20*, 329–364, doi:10.1146/annurev.ea.20.050192.001553.

Spear, F. S., and J. C. Markussen (1997), Mineral zoning, P-T-X-M phase relations, and metamorphic evolution of some Adirondack granulites, New York, *J. Petrol.*, *38*(6), 757–783, doi:10.1093/petroj/38.6.757.

Teagle, D. A. H., J. C. Alt, S. Umino, S. Miyashita, N. R. Banerjee, D. S. Wilson, and the Expedition 309/312 Scientists (2006), Superfast spreading rate crust 2 and 3, *Proc. Integrated Ocean Drill. Program*, *309/312*, 50 pp., doi:10.2204/iodp.proc.309312.2006. (Available at http://publications.iodp.org/scientific_prospectus/309_312/index.html)

Toplis, M. J., and M. R. Carroll (1995), An experimental study of the influence of oxygen fugacity on Fe-Ti oxide stability, phase relations, and mineral-melt equilibria in ferro-basaltic systems*J. Petrol.*, *36*(5), 1137–1170.

Toplis, M. J., G. Libourel, and M. R. Carroll (1994), The role of phosphorus in crystallisation processes of basalt: An experimental study, *Geochim. Cosmochim. Acta*, *58*(2), 797–810, doi:10.1016/0016-7037(94)90506-1.

Umino, S., S. Miyashita, F. Hotta, and Y. Adachi (2003), Along-strike variation of the sheeted dike complex in the Oman Ophiolite: Insights into subaxial ridge segment structures and the magma plumbing system, *Geochem. Geophys. Geosyst.*, *4*(9), 8618, doi:10.1029/2001GC000233.

VanTongeren, J. A., P. B. Kelemen, and K. Hanghoj (2008), Cooling rates in the lower crust of the Oman ophiolite: Ca in olivine, revisited, *Earth Planet. Sci. Lett.*, *267*(1–2), 69–82, doi:10.1016/j.epsl.2007.11.034.

Webb, S. C. (2008), Is there a deep hydrothermal circulation at the EPR?, *Eos Trans. AGU*, *89*(53), Fall Meet. Suppl., Abstract B21A-0327.

Wilson, D. S., et al. (2006), Drilling to gabbro in intact ocean crust, *Science*, *312*, 1016–1020, doi:10.1126/science.1126090.